ELECTRON CAPTURE INTO EXCITED STATES BY HELIUM IONS

L. WOLTERBEEK MULLER

3B

ELECTRON CAPTURE INTO EXCITED STATES BY HELIUM IONS

PROEFSCHRIFT

TER VERKRIJGING VAN DE GRAAD VAN DOCTOR IN DE WISKUNDE EN NATUURWETENSCHAPPEN AAN DE RIJKS-UNIVERSITEIT TE LEIDEN, OP GEZAG VAN DE RECTOR MAGNIFICUS DR. C. SOETEMAN, HOOGLERAAR IN DE FACULTEIT DER LETTEREN, TEN OVERSTAAN VAN EEN COMMISSIE UIT DE SENAAT TE VERDEDIGEN OP VRIJDAG 2 JULI 1971 TE KLOKKE 15.15 UUR

DOOR

LAMBERT WOLTERBEEK MULLER

GEBOREN TE DEN HAAG IN 1936

PROMOTOR: PROFESSOR DR. J. KISTEMAKER

This work has been done under supervision of

Dr. F.J. de Heer

CONTENTS

CHAPTER I

INTRODUCTION AND LITERATURE SURVEY

An important class of ion-atom collision processes are the rearrangement collisions: an electron, previously belonging to the target atom is taken over into a bound state by the projectile ion. In this category the dominating process will be the transfer of the electron into the ground state of the neutralized ion. Several proofs have indicated, however, that an appreciable fraction of the electrons is captures into an excited state of the projectile. This will also be shown experimentally in this work which is dedicated to an aspect of these collisions, which in general can be written as

$$X^+ + Y \rightarrow X^* + Y^+ \qquad (1)$$

The first symbol represents the fast projectile, the second one the slow target atom or ion.

Apart from its intrinsic interest this process is of importance in other fields: plasma and gas discharge physics, where it is one of the mechanisms of light emission and energy loss, and space and astrophysics. The related cross sections are roughly of the order of magnitude of the ones describing the direct excitation of the target atom:

$$X^+ + Y \rightarrow X^+ + Y^* \qquad (2)$$

In the study of the exchange process leading to excitation

more difficulties are encountered than with direct excitation. In the experiment one has to observe radiation from fast particles, which necessitates several precautions and in theory there are problems as to the choice of a set of wave functions and of the interaction potential during the collision.

For both reactions (1) and (2) at projectile energies of more than several tens of eV the scattering is strongly forwardly directed and the projectile energy is hardly reduced by energy transfer. Therefore total cross sections can be determined without the experiment being disturbed by scattering.

The laboratory equipment for these studies generally consists of an ion source at the acceleration potential wanted and a section containing the collision chamber and detector at earth potential (see fig. 1 of Chapter II).

Accelerations from about 20 eV up to several MeV have been used for atomic collisions. Mostly the ion beam, after leaving the source, is bent in a magnetic field region for selection of the proper ionic species before it enters into the collision chamber. Here the target is introduced, either as a second beam of particles or as a gas sufficiently dilute to ensure predominantly single collisions to happen for each projectile. Often the number of particles excited to a certain state is detected spectroscopically. This can be done when the atom decays by an optically allowed transition. For the detection of not decaying (metastable) states different techniques have to be applied.

Earlier optical experiments on electron capture were

carried out with protons as projectiles incident on noble gases and diatomic molecules. Electron capture into the n = 2 states was studied according to $H^+ + X \rightarrow H(2p) + X^+$. The 2p state atoms decay to the ground state emitting Lyman-α radiation (2p - 1s, 1216 Å). The other n = 2 state, 2s, is metastable because it cannot decay by an optically allowed transition. So the L_α intensity is a direct measure of the 2p capture rate. The cross section for 2p capture was measured for protons in the nergy range 2 - 35 keV [1]. The number of protons converted into H(2s) atoms can also be determined. When they are subject to an electric field the 2s states are mixed with 2p by the Stark effect. In a sufficiently strong field they decay completely, so that the additionally emitted L_α radiation yields the cross section for 2s capture[2]. As an example the results of H^+ on Ar from ref. 2 are shown in fig. 1.

As to the higher excited hydrogen states ($n \geqslant 3$), the formation of p states can be directly obtained from the intensity of the Lyman series (np - 1s) emission. This has been done by de Heer et al.[3] for 3p capture of protons on helium and neon leading to L_β radiation (3p - 1s, 1025 Å). The Lyman series measurements, however, suffer from great inaccuracies in the absolute magnitudes due to the difficult absolute calibration of detection equipment in the far ultraviolet. Further information has been obtained from the Balmer series ($n \geqslant 3 \rightarrow n = 2$) which is situated in the visible region, where the absolute calibration is less complicated. A different problem here is the hydrogenic fine structure, which causes each Balmer line to consist of three optical transitions (ns-2p, np-2s and nd-2p)

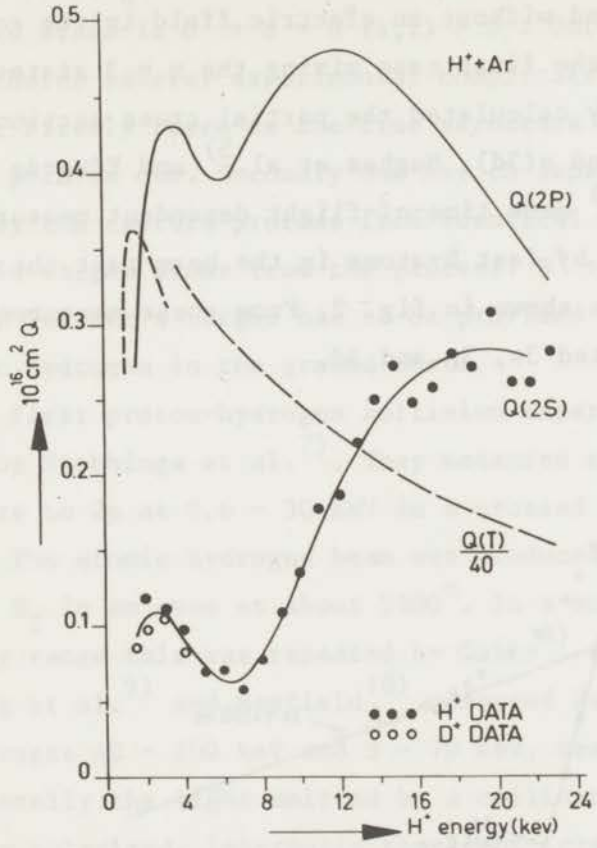

Fig.1. Electron capture to 2s and 2p by protons and deuterons on argon, as measured by Jaecks et al.[2], and total electron capture (T).

that cannot be resolved spectroscopically. Their resolution has to be accomplished by applying other techniques, based on the theoretical knowledge of the lifetimes and branching ratios of the hydrogen states. In this way the ratio of 3s, 3p and 3d in the total n = 3 capture have been determined. Andreev et al.[4] measured the intensities

of both Balmer-α (H_α, n = 3 → n = 2) and (L_β(3p - 1s) radiation with and without an electric field in the collision area, in the first case mixing the n = 3 states. From these data they calculated the partial cross sections σ(3s), σ(3p) and σ(3d). Hughes et al.[5] and Edwards and Thomas et al.[6] made time-of-flight dependent measurements of H_α emission by fast H-atoms in the beam past the collision region, as shown in fig. 2. From these measurements they deconvoluted 3s, 3p and 3d.

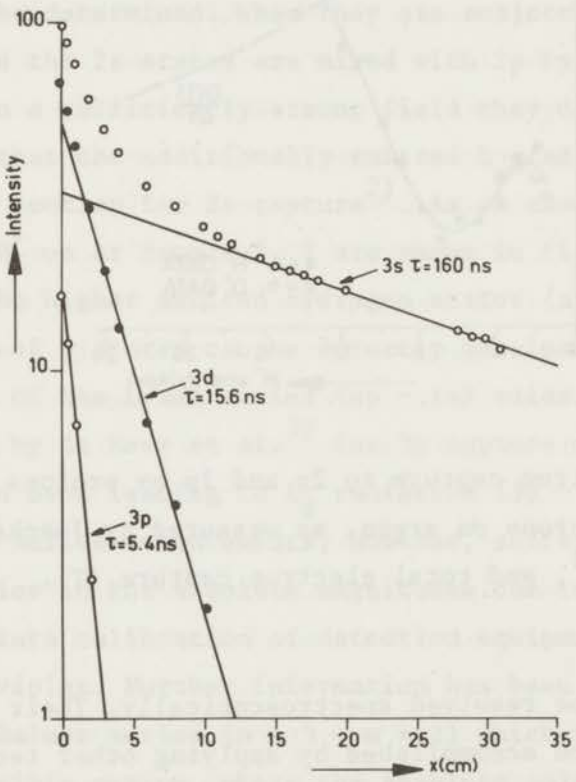

Fig.2. Dependence of H emission by a 20 keV proton beam in N_2 on the distance covered, as measured by Hughes et al.[5].

Typically, the most elementary process of capture to an excited state is $H^+ + H \rightarrow H^*(n,1) + H^+$. Unfortunately, in this choice several experimental complications are combined. Firstly there is the fine structure problem as already pointed out. Secondly one has to separate the radiation by the capture process from identical transitions by excited target atoms from the process: $H^+ + H \rightarrow H^+ + H^*(n,1)$. Further a target has to be provided consisting of atomic hydrogen in the ground state.

The first proton-hydrogen collision experiments were done by Stebbings et al.[7]. They measured excitation and capture to 2p at 0.6 - 30 keV in a crossed beam arrangement. The atomic hydrogen beam was produced by dissociating H_2 in an oven at about 2500°. In a more restricted energy range this was repeated by Gaily[8] (1-6 keV). Ryding et al.[9] and Bayfield[10] measured 2s capture in the ranges 40 - 200 keV and 3 - 70 keV, respectively.

Generally the light emitted by a colliding beam is partially polarized. Inherently the light intensity is not isotropic, but cylindrically symmetric around the beam axis. In the case of radiation of an atomic p-s transition there is a direct relation between the polarization fraction and the distribution among the three substates $m = 1,0,+1$ with regard to a quantization axis parallel to the beam[11,12]. Polarization of L_α radiation, H(2p-1s, 6365 Å) has been determined in angular dependent intensity measurements by Gaily et al. for protons incident on noble gases[13] and on hydrogen atoms[8] and by Teubner et al.[14] for protons on noble gases by application of a Brewster angle polarizer (0.6 - 24 keV).

In the total cross sections for electron capture into excited states by protons there are one or two maxima present in the covered energy region. In the process of H^+ on Ar as shown in fig. 1. there is a lower energy maximum occurring at the same energy as the maximum in the cross section for total electron capture, which is dominated by electron capture to the ground state. This suggests that these processes are coupled. Then there is a maximum at a few tens of keV. It can be considered as a resonance occurring when the effective collision time $\tau = \frac{a}{v}$ (a = effective interaction distance, v = relative velocity) is of the same order of magnitude as the reverse of the transition frequency $\nu = \frac{\Delta E}{h}$ (ΔE = change of internal energy). This is the so called Massey criterion. Maxima of this kind are found in all capture processes. Above this maximum the cross sections seem to decrease rapidly. This is clearly shown in the theoretical data on capture and excitation by H^+ on H, of which we cite the work of van den Bos and de Heer (Brinkman-Kramers approximation) [12], Wilets and Gallaher[15] and Cheshire et al.[16] (both close coupling impact parameter treatment) and Coleman and Trelease[17] (impulse approximation). When comparing capture and excitation for the same state it is seen from theory that at higher energies (about 100 keV and more, $v \geqslant 4.10^8$ cm/sec) capture cross sections decrease much faster than direct excitation ones with increasing impact energy. This is illustrated in fig. 3, taken from ref.[16] in which we have inserted correct values of Gaily.

For the capture experiment helium is simpler to handle than atomic hydrogen, both as target and as projectile.

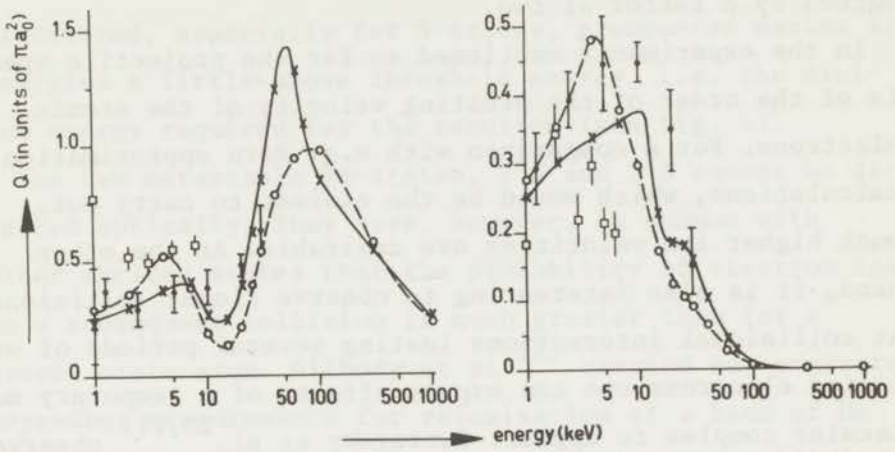

Fig.3a. 1s-2p excitation cross section. — X — 1s, 2s, 2p, 3s, 3p close coupling; -- O -- 1s, 2s, 2p close coupling; ⧫ experiment (Stebbings et al. corrected by Young et al.); □ experiment (Gaily and Geballe).

Fig.3b. 1s-2p charge exchange cross section. — X — 1s, 2s, 2p, 3s, 3p close coupling; -- O -- 1s, 2s, 2p close coupling; ⧫ experiment (Stebbings et al. corrected by Young et al.); □ experiment (Gaily and Geballe).

In the reaction $He^+ + He \rightarrow He^* + He$ all optical transitions can be separated spectroscopically, provided one is also able to distinguish between fast radiating particles (capture) and slow ones (direct excitation). Cross sections for charge transfer to most of the n = 3,4,5 states have been obtained by Head and Hughes[18] and de Heer et

al.[19] in the energy region 10 - 120 keV. Several maxima were found in either work, but the absolute values disagreed by a factor of two.

In the experiments mentioned so far the projectile speed is of the order of the orbiting velocity of the atomic electrons. For a comparison with e.g. Born approximation calculations, which would be the easiest to carry out, much higher ion velocities are desirable. At the other hand, it is also interesting to observe slower collisions. At collisional interactions lasting several periods of orbiting electrons one can expect effects of a temporary molecular complex to appear. Dworetsky et al.[20,21] observed the formation of excited helium states in He^+ colliding with He, 20 - 5000 eV.

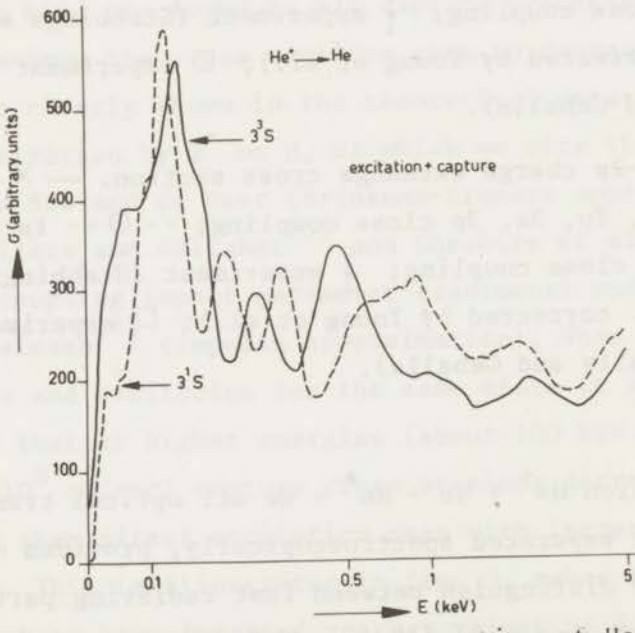

Fig.4. Cross sections for the creation of $He(3^1S)$ and $He(3^3S)$ states in collisions of helium ions on helium, as measured by Dworetsky et al.[20].

Radiation produced via electron capture and target excitation was not separated, but measured together. They discovered, especially for S-states, pronounced maxima at energies a little above threshold energy, i.e. the minimum energy required for the reaction (see fig. 4).

The two metastable He-states, 2^1S and 2^3S cannot be detected optically. They have, however, in common with other excited states that the probability of electron loss in a subsequent collision is much greater than for a ground state atom. Gilbody et al.[22] carried out pressure dependent measurements for reionization of a beam of He atoms, partially consisting of metastables and colliding with hydrogen. Thus they were able to determine the cross section for capture into the metastable states of He (2^1S and 2^3S) in the impact energy range of 80 - 250 keV. In a low energy collision experiment of He^+ on He (20 - 100 eV), MacVicar-Whelan and Borst[23] took advantage of the property of slow metastable atoms that by their surplus energy they are able to create secondary electrons from a metal surface.

In the present work we examine electron capture into several excited states by helium ions colliding with noble gases, according to

$$He^+ + X \rightarrow He^*(n^{1,3}S,\ n^{1,3}P,\ n^{1,3}D) + X^+,\ n = 3,4,5,6$$

The dependence of the capture process on principal and azimuthal quantum number and on the size of the target atom is investigated. Projectile energies ranged from 300 eV to 150 keV. At the lower energies (300 eV - 10 keV) also direct excitation of He by He^+ was measured, as an extension

of the work by de Heer and van den Bos[24]. This was thought to be interesting for a comparison with the capture process for He^+ on He.

In the light emission measurements a non-linear pressure effect of the light intensity was encountered, that was interpreted as an ionization of an excited projectile atom in a subsequent collision or as a redistribution among excited states. The effect was much greater than expected and was therefore more closely examined. Pressure dependent measurements were made out of which some collision cross sections for this process were derived.

REFERENCES

1) Pretzer, D., van Zijl, B. and Geballe, R., Phys.Rev. Letters 10 (1963) 340.

2) Jaecks, D., van Zijl, B. and Geballe, R., Phys.Rev. Letters 137 (1965) A340.

3) de Heer, F.J. and van Eck, J., Proc.IIIrd Int.Conf. Phys.Electr.At.Coll. 1963.

4) Andreev, E.P., Ankudinov, V.A. and Bobaskev, S.V., Soviet Phys. JETP 23, no.3 (1966) 375.

5) Hughes, R.H., Stigers, C.A., Doughty, B.M. and Stokes, E.D., Phys.Rev., A1, no.5 (1970) 1424.

6) Edwards, J.L. and Thomas, E.W., Phys.Rev. A2 (1970) 2346.

7) Stebbings, R.F., Young, R.A., Oxley, C.L. and Ehrhardt, H., Phys.Rev. 138 (1965) A1312.

8) Gaily, T.D., Ph.D.thesis, University of Washington, 1968.

9) Ryding, G., Wittkower, A.B. and Gilbody, H.B., Proc. Phys.Soc. 89 (1966) 547.

10) Bayfield, J.E., VIth Int.Conf.Electr.At.Coll. (1969) 118, M.I.T., Cambridge, U.S.A.

11) Percival, I.C. and Seaton, M.J., Phil.Trans.Roy.Soc. London A251 (1958) 113.

12) van den Bos, J. and de Heer, F.J., Physica 34 (1967) 333 and Physica 40 (1968) 161.

13) Gaily, T.D., Jaecks, D.H. and Geballe, R., Phys.Rev. 167, no.1 (1968) 81.

14) Teubner, P.J.O., Kauppila, W.E., Fite, W.L. and Girnius, Phys.Rev.A. 2 (1970) 1763.

15) Wilets, L. and Gallaher, D.F., Phys.Rev. 147, no.1 (1966) 13.

16) Cheshire, I.M., Gallaher, D.F. and Taylor, A.J., J. Phys.B.At.Mol.Phys. 3 (1970) 813.

17) Coleman, J.P. and Trelease, S., J.Phys.B.At.Mol.Phys. 1 (1968) 172.

18) Head, C.E. and Hughes, R.H., Phys.Rev. 139 (1965) A1392.

19) de Heer, F.J., Wolterbeek Muller, L. and Geballe, R., Physica 31 (1965) 1745.

20) Dworetsky, S.H., Novick, R., Tolk, N. and Smith, W. W., Phys.Rev.Letters, 18 (1967) 939.

21) Dworetsky, S.H., Novick, R., Phys.Rev.Letters 23 (1969) 1484.

22) Gilbody, H.G., Browning, R., Levy, G.J., McIntosh, A.I. and Dunn, K.F., J.Phys.B.Atom.Mol.Phys. 1 (1968) 863.

23) Macvicar-Whelan, P.J. and Borst, W.L., Phys.Rev. A1, (1970) 314.

24) de Heer, F.J. and van den Bos, J., Physica 31 (1965) 365.

ELECTRON CAPTURE INTO EXCITED STATES BY HELIUM IONS INCIDENT ON NOBLE GASES

Synopsis

An experimental study has been made of capture of an electron into an excited state by helium ions incident on helium, neon, argon, krypton and xenon in the energy range of 0.3 to 150 keV. Cross sections have been determined for capture into singlet and triplet He I levels with principal quantum numbers n varying between 3 and 6 by means of observation of the resulting emission of light. Pronounced oscillations are found in the cross sections, especially for He^+ on He and Ne. If we compare the oscillations for He^+ on He for capture and excitation leading to the same final excited state on the projectile or the target atom, then these oscillations often have an antiphase for capture and excitation. This is explained by the interference of gerade and ungerade scattering in the intermediate excited He_2^+ molecule-ion. Oscillations in excitation + capture cross sections for He^+ on He and in capture cross sections for He^+ on other atoms may be connected with pseudo curve crossing of potential curves in intermediate molecular complexes and resulting interference effects between different modes of scattering.

1. *Introduction.* In the present work we investigate collisions between He ions and noble gas atoms in which an electron is captured into an excited state. This is important to understand the experimental results on total electron capture, where the exchange of charge is measured, in more detail. The processes studied here are

$$He^+ + X \rightarrow He^* + X^+, \qquad (1)$$

where X stands for one of the noble gas atoms. The resulting radiation from He* is detected optically and the corresponding capture cross sections are evaluated.

We shall summarize previous experimental work on these processes: Formation of 2^1P and 3^1P He levels was measured by de Heer *et al.*[1]) for (5–35 keV) He^+ ions on H_2, He, Ne and Kr. Head and Hughes[2]) measured cross sections for the production of most of the $n = 3$ and $n = 4$ states of He for (20–120 keV) He^+ ions on He, N_2 and O_2. For (5–90 keV) He^+ ions on He similar measurements have been carried out by de Heer *et al.*[3]) for $n = 3$–6 states of He. In a range of relatively small energy (20–5000 eV)

relative capture cross sections ($n = 2$–4) have been measured by Dworetsky *et al.*[4,5]) for He^+ on He and by Tolk and White[6]) for He^+ on Ne. These results show a pronounced structure for the cross sections as a function of impact energy, which is attributed to pseudocrossing of potential energy curves of the intermediate molecular complex.

For reasons of completeness we mention some nonoptical measurements dealing with capture of electrons into metastable He states: Gilbody *et al.*[7]) and Miers *et al.*[8]) investigated this process for He^+ ions on a variety of gases by beam attenuation techniques. Peterson *et al.*[9]) studied the production of metastables in near-resonant reactions by charge-changing measurements.

The present work is an extension of the experimental studies of our group described in ref. 3, covering a wider energy range (0.3–150 keV) and using several target atoms (He, Ne, Ar, Kr and Xe).

2. *Introduction of the cross sections involved.* For the definition of different physical quantities we use the same notation as in ref. 10. We have a parallel beam of I/e singly charged ions passing per second through a gas with a concentration of N atoms per cm^3. When the ion captures an electron from a target particle an atom in a certain state i will be formed in the beam. If σ_i is the cross section for this process, n_i the number of beam particles per cm beam length being in state i and A_{ij} the radiative transition probability from state i to j, then

$$\frac{dn_i}{dt} = \sigma_i N I/e + \sum_{k(>i)} n_k A_{ki} - n_i \sum_{j(>i)} A_{ij}. \tag{2}$$

The rate of change of n_i in the beam is equal to the algebraic sum of direct creation of state i by collisions plus cascade from higher states k to i minus the decay from i to lower states j.

Both the beam intensity and the target-gas density are chosen sufficiently low so that secondary collision effects are negligible. So, if beam ions capture an electron into an excited state they can, in good approximation, be supposed to decay before a second collision occurs (except for the metastable states).

In our energy range we suppose that variations in the beam velocity v due to inelastic processes are negligible.

We introduce a position coordinate $x = vt$, representing the distance which a particle has travelled through the gas. We have

$$\frac{dn_i(t)}{dt} = v \frac{dn_i(x)}{dx}. \tag{3}$$

In our case, where we deal with fast excited beam particles, n_i depends strongly on x in contrast to the case of excited target atoms for which $dn/dt = 0$. The emission cross section σ_{ij} has to be defined therefore in more detail. It corresponds to the number of photons $i \rightarrow j$ emitted per second

along an observation length L between $x = l$ and $x = l + L$ (see also fig. 6). This number is

$$\int_{l}^{l+L} n_i(x)\, A_{ij}\, \mathrm{d}x = \sigma_{ij} N L I / e. \tag{4}$$

The relation between σ_{ij} and σ_i can be derived from eqs. (2), (3) and (4) and will be discussed in section 6.

The cross section σ_{ij} is determined by measuring the intensity of the light of the corresponding $i \rightarrow j$ transition emitted by the beam particles; the transitions observed are listed in table I.

3. *Description of the apparatus.* 3.1. The accelerators. For the production of a beam of helium ions four accelerators have been used. Three of them are of a conventional type with an energy range from 0.3 to 10, 5 to 35 and 30 to 150 keV, respectively. They have been described by van Eck *et al.*[11]) and van den Bos *et al.*[12]) and consist of an ion source (uno- or duoplasmatron), an extraction electrode, an electrostatic lens system and an analysing magnet. While in these three instruments the beam was only accelerated, in the fourth one, constructed during the course of this investigation, an acceleration–deceleration system was applied. It will be described here in more detail (see fig. 1). This instrument (0.3–40 keV) has the same constituents as the other accelerators but is different in that the section containing extraction electrode, electrostatic lenses L_1, L_2 and L_3 and the magnetic analyser is insulated from earth and connected to the extraction electrode E and electrode F. They are all connected to the negative voltage V_1 of a floating 40 kV supply, the ion source to the positive voltage V_2. A third voltage V_0 which is schematically represented by the tap of a voltage divider and adjustable between V_1 and V_2 is grounded. So are the pumping chamber and collision chamber including the deceleration plate D. It follows from the scheme in fig. 1 that the ions are accelerated by the voltage $V_1 - V_2$ between the ion source and the extraction electrode E and decelerated between electrode F and ground plate D by the voltage $V_0 - V_2$. So the final beam energy corresponds to an acceleration of $V_1 - V_0$.

The practical advantages of this type of accelerator are: only one parameter, V_0, has to be changed for energy selection, thus making the apparatus suitable for continuous energy-dependent measurements; a constant efficiency of ion extraction is obtained; the space-charge effects are reduced by the relatively high speed of the beam through the accelator.

3.2. The collision chamber and optical equipment. After deceleration the beam passes through a pumping chamber and enters into the collision chamber via a collimator C, which is movable into the beam direction (see fig. 1). By changing the position of collimator C, we vary the

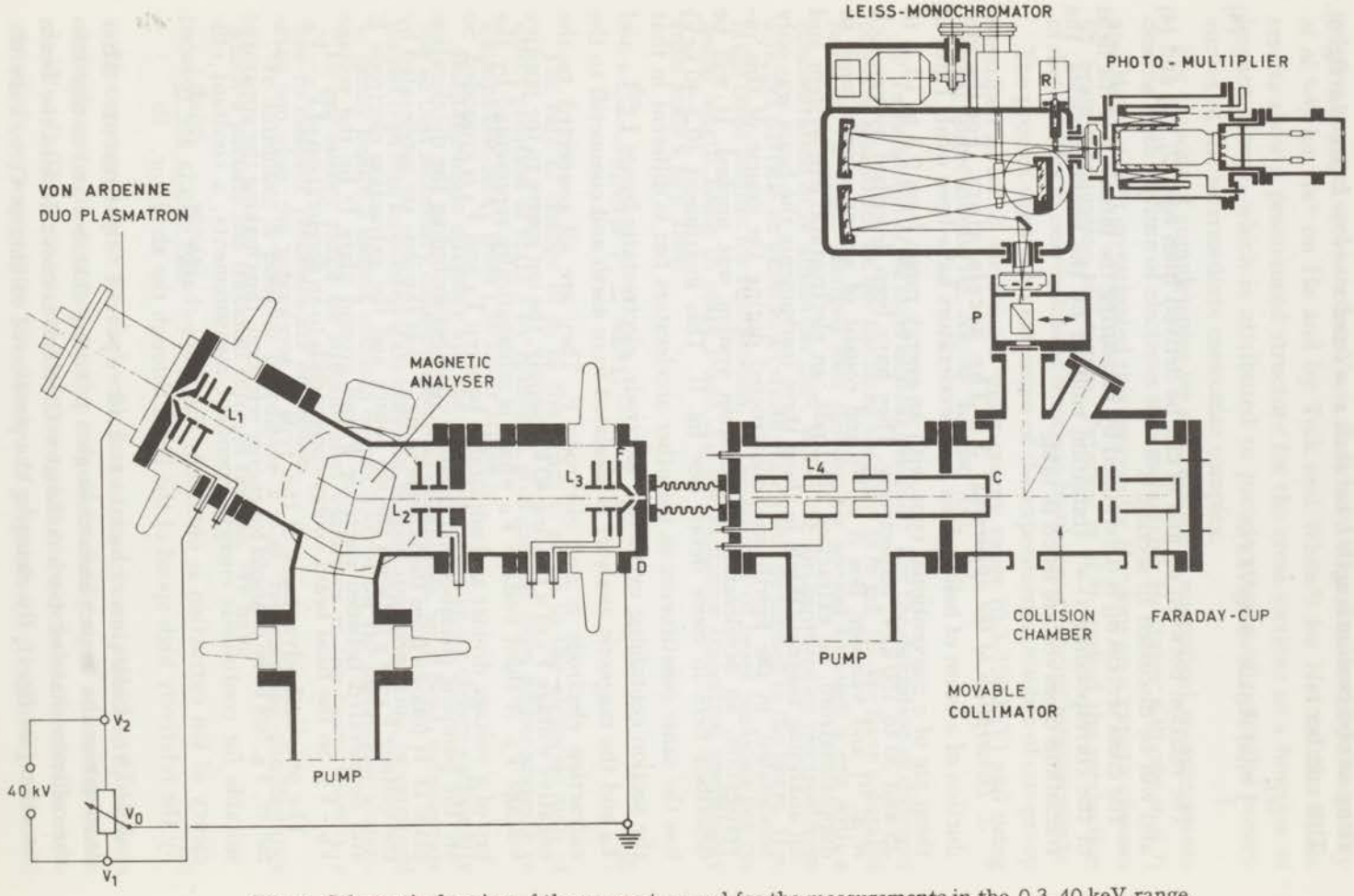

Fig. 1. Schematic drawing of the apparatus used for the measurements in the 0.3–40 keV range.

path length l (see eq. (4)) through the gas before the observation room of length L. This is a useful device for the study of the effect of the finite lifetime of the levels of the excited beam particles (He atoms) on the radiation process (see section 9.1). The radiation from the beam is observed by a monochromator and its current is measured in a Faraday cup. In front of the cup two rings are mounted, the first of which is used to check whether the beam diameter is sufficiently small and the second one to suppress secondary electrons possibly emerging from the cup. The beam currents varied between 1 and 100 μA, using a beam diameter of about 4 mm.

The target gas is introduced into the collision chamber via a needle valve. It flows via collimator C into the pumping chamber, where it is pumped away by an oil diffusion pump backed by a rotary pump. In the pumping chamber the pressure is about 300 times smaller than in the collision chamber. The gas pressure used in the collision chamber varies between about 2×10^{-4} and 10^{-3} torr. A liquid air trap is used in the collision chamber to condense organic vapours and water vapour. Only in the case of Xe target gas it cannot be used.

The gas pressure in the collision chamber is monitored by an ionization manometer and measured by a McLeod gauge provided with a liquid air trap. Precautions were taken in its construction to avoid the diffusion effect of mercury vapour (see Ishii and Nakayama[13]) in the same way as in ref. 14.

The radiation produced by the excited beam particles is measured by means of a 30 cm radius Leiss monochromator ($f \approx 7$) in which the original prism has been replaced by a reflection grating of Bausch and Lomb with 1800 lines per mm, thus forming a Czerny–Turner mounting. The dispersion is about 18 Å per mm. Slit widths between 1.5 and 0.1 mm are used. The photons are detected with an E.M.I. photomultiplier at the exit slit; for wavelengths between 2800 and 6000 Å the 6256 S type is used, for longer wavelengths up to 7300 Å the 9558 B type. Both detectors are cooled with freon or Peltier elements in order to decrease the dark current. Changes in the photomultiplier amplification were detected by checking during every measurement (the intensity calibration included) the signal from a sample of radioactive fluorescent material (R), which is mounted inside the monochromator and can be placed in front of the exit slit.

The monochromator has been mounted to the collision chamber at an angle of either 90° or 60° with respect to the ion beam. In the case of 60° it is possible in symmetrical combinations (*i.e.* He^+ on He) to separate the radiation of the same transitions of the fast atom and the target atom by making use of the Doppler shift in the radiation of the beam particles. For other targets this is also necessary when there is a coincidence in wavelengths for transitions in the helium and target atom.

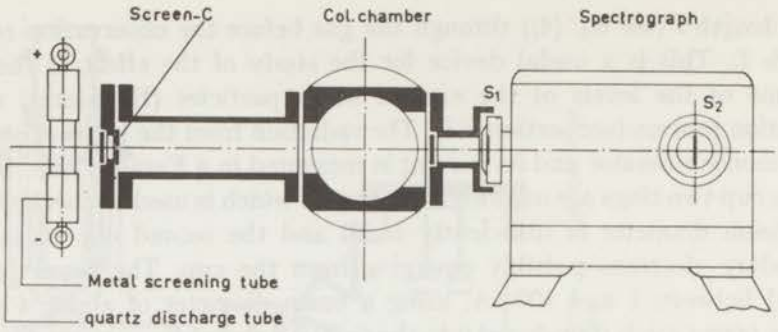

Fig. 2. The arrangement used for the determination of the quantum yield of the optical equipment with the mercury standard lamp.

4. *The intensity calibration of the optical equipment.* The sensitivity of the monochromator with photomultiplier has been determined by means of two light standards, a tungsten ribbon lamp and an ultraviolet mercury standard lamp. These lamps were mounted to the collision chamber at the opposite side of the monochromator (see fig. 2). Their radiation passes through quartz windows at either side of the chamber.

The tungsten ribbon-lamp emits a continuous spectrum, the intensity of which has been measured as a function of wavelength and ribbon temperature by De Vos[15]). The calibration procedure with this standard has been described previously[11,12,16]). The standard could only be used down to about 3000 Å as a consequence of the sharp decrease of the emission by the hot tungsten filament towards lower wavelengths and the relative increase of scattered light.

The calibration was extended to about 2700 Å by means of a mercury ultraviolet standard lamp. The spectrum consists of spectral lines and a continuum. The intensities of both are known from measurements by Krefft *et al.*[17]), who introduced the lamp, and by van Stekelenburg[18]). These intensity data refer to the radiation from the entire quartz discharge tube. For attenuation of its large radiation intensity a narrow horizontal diafragm C of 0.01 mm was placed in front of the vertically mounted lamp. A check was made concerning the uniformity of the radiation intensity with respect to the location of the lamp. A good uniformity was found in the longitudinal direction of the quartz tube only, so that the diafragm C had to be chosen sufficiently wide to cover the whole width of the discharge tube.

In the overlapping wavelength region a difference of about 10% was found in the sensitivity of the optical equipment measured with the tungsten and the mercury standards. Since we have more confidence in the accuracy of the tungsten standard, we normalized the mercury standard data to the tungsten ones.

We have to consider that in both calibrations the parts of the grating

and photomultiplier which are illuminated are much smaller than in the case of the beam experiments. The calibration with the ribbon lamp was repeated therefore in a different arrangement with lenses, by means of which the opening angle of the light entering the monochromator was made much larger; almost the entire grating was illuminated. The sensitivity found in this setup appeared to deviate by less than 5% from that found in the arrangement of fig. 2. This is consistent with the test described by Van den Bos *et al.*[12]), who mounted an extra diaphragm in the collision chamber between the ion beam and the monochromator, thus illuminating the same small area of the grating in the beam and calibration experiment. They found a deviation smaller than 3% for the sensitivity with respect to the usual arrangement.

5. *Determination of the emission cross sections.* We have mentioned in section 2 (eq. (4)) that the total number of photons $i \rightarrow j$ emitted per second by the beam is given by

$$\sigma_{ij}\, NLI/e = \int_{l}^{l+L} n_i(x)\, A_{ij}\, \mathrm{d}x, \tag{4}$$

where L is, as before, the observation length.

In the case of isotropic emission of radiation the number of photons entering the monochromator slit per second is

$$(\omega/4\pi)\, \sigma_{ij}\, NLI/e, \tag{5}$$

ω being the solid angle under which the light enters the monochromator (slit) from an emitting particle in the beam. This solid angle is approximately constant over the length L.

The corresponding signal S of the photomultiplier at the exit slit of the monochromator can be given by

$$S = k(\lambda)(\omega/4\pi)\, \sigma_{ij}\, NLI/e, \tag{6}$$

or

$$\sigma_{ij} = \frac{4\pi}{\omega}\, \frac{S}{NLK(\lambda)\, I/e}, \tag{7}$$

$k(\lambda)$ is the sensitivity of the monochromator with photomultiplier in ampere second per photon.

The determination of the different quantities in the right hand side of eq. (7) has already been described in sections 3.2 and 4. We just add a few remarks. The signal S of the emission lines is measured at a pressure of about 5×10^{-4} torr. The background pressure in the collision chamber is about 5×10^{-6} torr. Contributions to S due to this residual gas are measured and subtracted from it. The beam current I is determined under vacuum

conditions, because when the collision chamber is filled with target gas the current of ions at the Faraday cup diminishes as a consequence of the electron capture process. It is assumed that the beam current entering the collision chamber is the same under vacuum conditions and when gas is present there. The gas density N follows from the pressure measurement with the McLeod and the temperature (about 293 K). The quantities ω and L follow from the geometry of the setup. At an entrance slit of the monochromator of 8 mm $\times$ $\frac{1}{2}$mm, ω is about 1.1×10^{-3} sterad and L is about 3 cm. The distance between the ion beam and the entrance slit is about 18 cm.

Eq. (7) is still incomplete in so far that two correction factors have to be added, one (P) due to the polarization of the radiation and one (D) due to the broadening of the emission lines by the Doppler effect, so that instead of eq. (7) we get

$$\sigma_{ij} = \frac{4\pi}{\omega} \frac{S}{NLK(\lambda)\, I/e} \cdot P \cdot D. \tag{8}$$

The determination of P and D will be described in sections 7 and 8.

6. *The calculation of the capture cross sections σ_i from the emission cross sections σ_{ij}.* In order to establish the relation between σ_i and σ_{ij} we first solve $n_i(x)$ from eqs. (2) and (3). When omitting the cascade term $\sum_{k(>i)} n_k A_{ki}$ in (2) we obtain:

$$n_i(x) = \sigma_i N(I/e)\, \tau_i[1 - \exp(-x/x_i)]; \tag{9}$$

here $x_i = v\tau_i$, and $\tau_i = 1/\sum_{j<i} A_{ij}$, the mean lifetime of state i. Substituting (9) into (4) we get after some evaluation

$$\sigma_i = \frac{\sigma_{ij}}{A_{ij}\tau_i} \Bigg/ \left[1 - \frac{x_i}{L} \exp(-l/x_i)(1 - \exp(-L/x_i))\right]. \tag{10}$$

$A_{ij}\tau_i$ is the branching ratio, the fraction of states i that decay to j. The factor between brackets, further abbreviated as $1 - F_i(x)$ is called the lifetime correction factor and represents the fraction of excited fast particles that decay in the observation region before leaving it. For $l = 0$ it becomes equal to the expression presented by Hanle and Voss[19]).

Now we apply a first- order cascade correction by solving $n_i(x)$ from eqs. (2) and (3) with inclusion of the term $\sum_{k>i} n_k A_{ki}$ and substituting $n_k(x)$ according to eq. (9) without its own cascade. For $n_i(x)$ we now obtain

$$n_i(x) = (I/e)\, N\tau_i \Bigg[(\sigma_i + \sum_{k(>i)} \sigma_k A_{ki}\tau_k)(1 - \exp(-x/x_i)) - \sum_{k(>i)} \sigma_k A_{ki}\tau_k x_k \frac{\exp(-x/x_k) - \exp(-x/x_i)}{x_k - x_i}\Bigg], \tag{11}$$

which after substitution into (4) leads to

$$\sigma_i = (\sigma_{ij}/A_{ij}\tau_i) \Big/ \left[\left(1 + \sum_{k(>i)} \frac{\sigma_k}{\sigma_i} A_{ki}\sigma_k\right)(1 - F(x_i) - \sum_{k(>i)} \frac{\sigma_k}{\sigma_i} A_{ki}\tau_k x_k \frac{F(x_k) - F(x_i)}{x_k - x_i}\right]. \quad (12)$$

In practice σ_i and σ_k are calculated first without cascade correction from σ_{ij} by means of eq. (10), including the lifetime correction which often is very large. Next these results are substituted into the right-hand side of eq. (12) giving the first-order cascade corrected values for σ_i.

In the calculation of the cascade contributions, all levels with quantum numbers up to $n = 6$ have been taken into account. An extrapolation according to an n^{-3} dependence of the cross section was applied for the determination of the cascade from those levels that could not be measured. Higher terms could be neglected as their cascade contribution becomes relatively small.

Regarding the atomic transition probabilities A_{ij} two sets of theoretically calculated results exist for the most important s–p and p–d transitions; these are the ones of Trefftz *et al.*[20]) and the ones tabulated by Gabriel and Heddle[21]). The latter ones were obtained from calculations of Dalgarno and Lynn[22]), Dalgarno and Stewart[23]) and by application of the Coulomb approximation of Bates and Damgaard[24]). Here we have used the numbers of Gabriel and Heddle. They are closer to some accurate results more recently obtained by Schiff and Pekeris[25]) and Weiss[26]) than those of Trefftz *et al.*[20]); the difference is generally 5% or less, except for the 4^3P–2^3S transition where a deviation of 10% exists. For 4^3S–2^3P no accurate calculation of A_{ij} exists and the difference between values of Gabriel and Heddle and Trefftz amounts to 13%. The influence of an error in the lifetime on the evaluated cross sections will be discussed further on (see section 10).

7. *Polarization of the radiation.* The polarization of the radiation is determined by measuring the ratio of the signals $S_{//}$ and $S_{\perp}$, representing the components of S in eq. (8) with electric vectors parallel and perpendicular to the ion beam respectively, when observing at an angle of 90° with respect to the ion beam. These signals are measured by means of a Glan Thompson prism (P) in front of the monochromator (see fig. 1). Then the ratio of the intensities $I_{//}$ and $I_{\perp}$ of the components can be evaluated by

$$\frac{I_{//}}{I_{\perp}} = \frac{S_{//}}{S_{\perp}} \cdot \frac{K_{\perp}(\lambda)}{K_{//}(\lambda)}. \quad (13)$$

$K_{//}(\lambda)$ and $K_{\perp}(\lambda)$ are the quantum efficiencies for the polarized light compo-

nents and are different in our setup due to the polarizing effect of the reflection grating of the monochromator.

Often the polarization fraction Π is given, defined as

$$\Pi = \frac{I_{//} - I_{\perp}}{I_{//} + I_{\perp}}. \tag{14}$$

For an observation angle Θ different from 90° (in our case 60°) we maintain the same definition for $I_{\perp}(\Theta)$, but $I_{//}(\Theta)$ is defined now as the component with electric vector perpendicular to the observation direction and in the plane of the ion beam and observation direction (see refs. 3 and 12). According to Smit[27]) we have

$$\begin{aligned} I_{\perp}(\Theta) &= I_{\perp}, \\ I_{//}(\Theta) &= I_{\perp} \cos^2\Theta + I_{//} \sin^2\Theta. \end{aligned} \tag{15}$$

From the polarization measurements at 60°, carried out in those cases where we want to separate spectral lines with (almost) coinciding wavelengths by means of the Doppler shift (see section 3.2), the polarization at 90° is found by

$$\frac{I_{//}}{I_{\perp}} = \frac{4}{3}\,\frac{I_{//}(60°)}{I_{\perp}(60°)} - \frac{1}{3}. \tag{16}$$

We can give now the expression for the correction factor P of eq. (8), due to the polarization of radiation. We introduce the symbols B and C given by

$$B = \frac{K_{//}(\lambda)}{K_{\perp}(\lambda)} \qquad \text{and} \qquad C = \frac{I_{//}}{I_{\perp}}. \tag{17}$$

Then P can be written as the product of two factors: $P_1(C, \Theta)$ is due to the anisotropy of the radiation emitted by the beam and $P_2(B, C)$ is due to the polarizing effect of the monochromator. It can be derived that

$$P_1(C, \Theta) = \frac{3 - \Pi}{3(1 - \Pi \cos^2 \Theta)}, \tag{18}$$

$$P_2(B, C) = \frac{(1 + B)(1 + C)}{2(BC + 1)}, \tag{19}$$

and for $\Theta = 90°$

$$P = P_1 P_2 = \frac{(1 + B)(2 + C)}{3(BC + 1)}. \tag{20}$$

8. *The effect of Doppler broadening of the emission lines.* In the considerations about light intensity measurements it was assumed that every

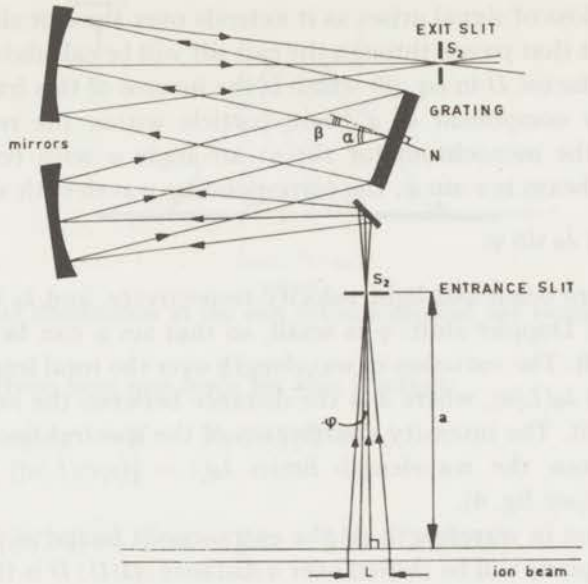

Fig. 3. The ion beam and the arrangement for optical observation.

part of the excited beam in the observation region gives rise to radiation of the same wavelength into the monochromator. However, due to the velocity of the radiating particles a Doppler shift is introduced. Because of the finite acceptance angle of the monochromator the Doppler shift, which depends on the velocity component of the radiating particle in the direction to the monochromator slit, varies with the position of the radiating particle of the beam in the observation region. This variation of Doppler shift leads to a Doppler broadening of the emission lines. The image of the entrance slit opening, as it is focussed in the exit slit area, is broadened accordingly.

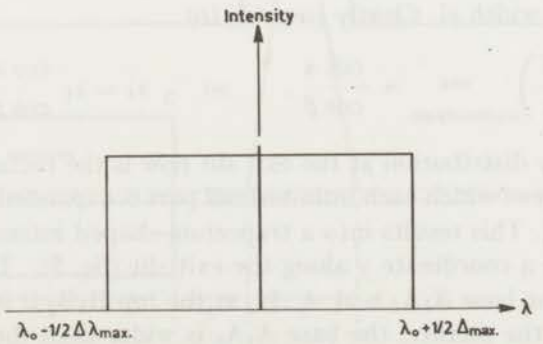

Fig. 4. Broadening of a spectral line emitted by the beam particles in the observation region.

An additional loss of signal arises as it extends over the exit slit edges. The fraction of light that passes through the exit slit will be calculated and yields the correction factor D in eq. (8) which is the inverse of this fraction.

The velocity component of a beam particle within the region L that radiates into the monochromator slit at an angle φ with respect to the normal to the beam is $v \sin \varphi$, the corresponding wavelength shift is

$$\Delta\lambda = (v/c)\, \lambda_0 \sin \varphi.$$

Here v and c are beam and light velocity respectively, and λ_0 is the wavelength without Doppler shift. φ is small, so that $\sin \varphi$ can be replaced by $\tan \varphi$ (see fig. 3). The variation in wavelength over the total length L is then $(\Delta\lambda)_{\max} = (v/c)\, \lambda_0(L/a)$, where a is the distance between the ion beam and the entrance slit. The intensity distribution of the spectral line λ_0 is almost constant between the wavelength limits $\lambda_0(1 - \frac{1}{2}(v/c)(L/a))$ and $\lambda_0(1 + \frac{1}{2}(v/c)(L/a))$ (see fig. 4).

By a variation in wavelength $\Delta\lambda$ the entrance slit image as it is focussed in the exit slit plane will be shifted over a distance $\Delta\lambda/D$; D is the dispersion and follows from the grating formula for the first order diffraction

$$\lambda = \mathrm{d}(\sin \alpha + \sin \beta), \tag{21}$$

where d is the grating constant and α and β the diffraction angles:

$$D \equiv f\left(\frac{\partial\beta}{\partial\lambda}\right)_{\alpha=\text{constant}} = \frac{f}{d \cos \beta}, \tag{22}$$

where f is the focal length of the concave mirror.

The image broadening by the Doppler effect becomes

$$\Delta y = \frac{\Delta\lambda_{\max}}{d \cos \beta} = \frac{\lambda_0 v L}{c a d \cos \beta}. \tag{23}$$

For each discrete wavelength λ the entrance slit of width s_1 is focussed as an image of width s_1'. Clearly (see ref. 16)

$$\frac{s_1'}{s_1} = \left(\frac{\partial\beta}{\partial\alpha}\right)_{\lambda=\text{constant}} = \frac{\cos \alpha}{\cos \beta}, \qquad \text{so} \qquad s_1' = s_1 \frac{\cos \alpha}{\cos \beta}. \tag{24}$$

The intensity distribution at the exit slit now is the rectangular distribution of width Δy of which each infinitesimal part is expanded homogeneously over a width s_1'. This results into a trapezium-shaped intensity distribution with respect to a coordinate y along the exit slit (fig. 5). The width of the trapezium at the base A_1A_2 is $s_1' + \Delta y$, at the top B_1B_2 it is $|s_1' - \Delta y|$.

When, as in the picture, the base A_1A_2 is wider than the exit slit s_2 the fraction of the light passing through the slit is equal to the ratio of the areas $C_1B_1B_2C_2D_2D_1$ and $A_1A_2B_2B_1$. After some planimetric calculation which

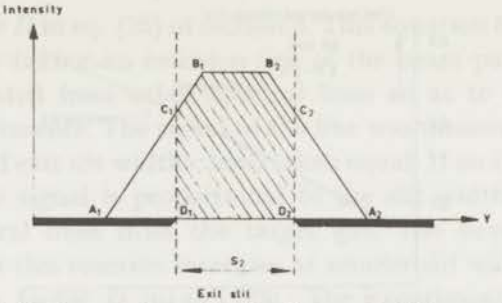

Fig. 5. Intensity distribution at the exit slit of a spectral line emitted by the beam.

will not be given here one finds for this fraction:

$$(1/D) = s_2/\Delta y \qquad \text{if} \qquad \Delta y \geq \tfrac{1}{2}(s_1' + s_2)$$

and else

$$(1/D) = (1/2s_1')\,[s_1' + s_2 - \tfrac{1}{2}\Delta y - \tfrac{1}{2}(s_2 - s_1')^2/\Delta y]. \tag{25}$$

9. *Experimental checks on the corrections due to lifetime and Doppler broadening.* 9.1. The lifetime correction. In order to investigate whether the lifetime correction represented by eq. (10) is correct an experimental check was carried out. Measurements were done on the light emission with variation of the parameter l of eq. (10). This experiment was done for the transitions with upper levels 4^1S, 4^3S, 5^3S and 5^3P, because these levels have relatively long lifetimes in combination with a small

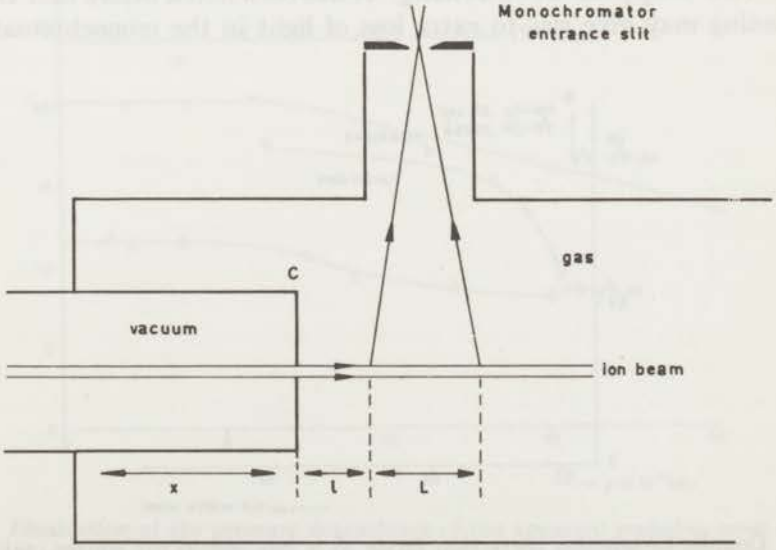

Fig. 6. Schematic view of the collision chamber and the movable beam collimator.

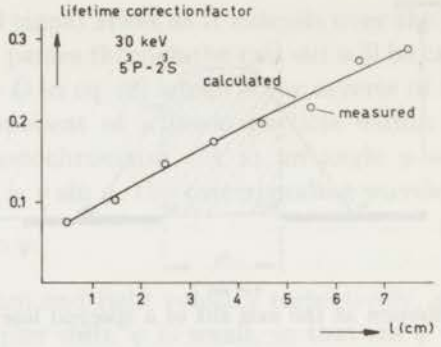

Fig. 7. Lifetime correction factor as a function of l, calculated and measured.

perturbation by cascade. The length l was varied by changing the position x of the movable collimator C (see fig. 6). The emission measured as a function of l is compared with calculated relative values. The comparison for 5^3P–2^3S is shown in fig. 7.

In the approach presented in eq. (10) and further on it was supposed that at the beam entrance opening of the collision chamber (see fig. 6) the target gas pressure suddenly increases from zero to the value it has all over the chamber. There is, however, a gradual pressure fall from the vicinity of this opening to the end of the collimator cylinder. By applying a gas kinetic model for the pressure distribution we calculated the contribution to the radiation in the region L from collisions occurring in this region and found it to be negligible.

9.2. The Doppler broadening. It has been noted before that Doppler broadening may give rise to extra loss of light in the monochromator, as

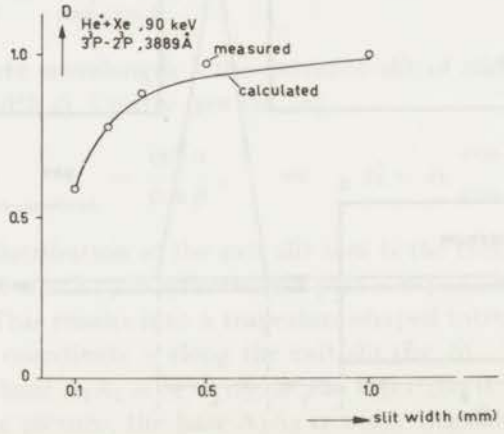

Fig. 8. Doppler-broadening correction factor as a function of slit widths, calculated and measured.

given by the factor D in eq. (25) of section 8. This equation has been checked experimentally by taking an emission line of the beam particles, that was sufficiently separated from other spectral lines so as to allow slit-width dependent measurements. The signal of the line was measured as a function of the entrance and exit slit widths, both taken equal. If no Doppler broadening is present, the signal is proportional to the slit width. This has been verified for spectral lines from the target gas. The deviation from the proportionality for this reaction increases at smaller slit widths and is given by the correction factor D in eq. (25). The experimental values fitted reasonably well to the calculated ones if s_1' was taken 0.05 mm larger than calculated (see eq. (25)) as shown in fig. 8. The order of magnitude of this addition corresponds to the observed curvature of the slit image due to spherical aberration of the concave mirrors.

10. *Pressure effects due to electron loss processes.* The pressure effect observed in the measurements above 30 keV is shown in fig. 9. At pressures of about 6×10^{-4} torr a deviation started from the linear relation between the light intensity and the gas pressure. The effect increased for larger values of distance l (see fig. 6) and with the lifetime of the excited states. This effect is caused by ionization of the excited projectile atom before it radiates. For excited hydrogen atoms Thomas *et al.*[28]) have recently made an experimental study of this process. For the relevant He* states the excited

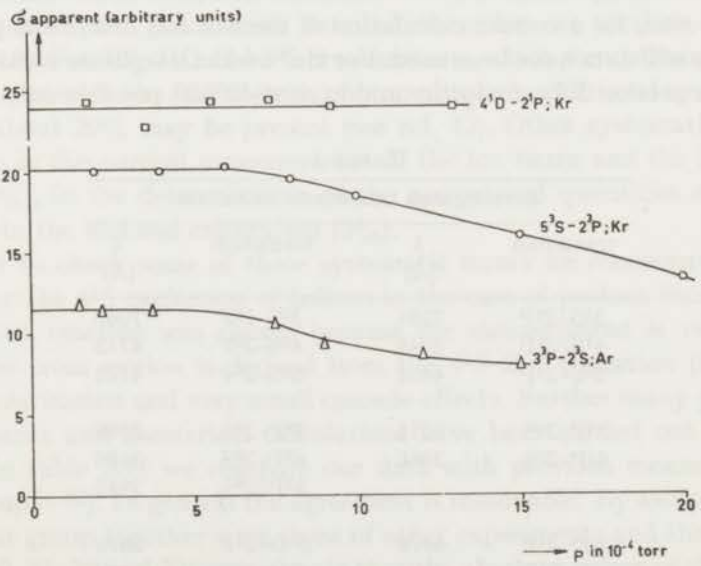

Fig. 9. Illustration of the pressure dependence of the apparent emission cross section at 90 keV in the case of He^+ incident on Ar and Kr for capture into 4^1D, 3^3P and 5^3S states.

electron has a binding energy of only 0.7–1.7 eV, so that loss of this electron can be a process with a large cross section. At 90 keV for He (5^3S) colliding with Kr we find the cross section for this electron loss process to be about 3×10^{-15} cm^2. This order of magnitude is confirmed by the measurements of Gilbody *et al.*[7]) who measured the electron loss from metastable He atoms colliding with H_2 molecules. At 90 keV they found that the cross section reaches a maximum of about 0.8×10^{-15} cm^2. When keeping in mind that the metastable 2^1, ^3S states have a greater binding energy (about 4 eV) our cross sections for electron loss may very well be larger.

A pressure effect can also occur by electron capture into the ground state leading to a decrease of the number of active ions in the beam. This effect would have a maximum at an energy where the ground-state capture cross section has a maximum being far below 90 keV as found for the ionization of the excited He atoms.

11. *Results and error discussion.* The investigated transitions in helium are given in table I. The cross sections for capture into singlet and triplet S, P and D states are shown in tables II–VI, the polarization of the radiation is given in tables VII and VIII. In the symmetrical combination of He^+ on He the cross sections for excitation of the target atom have also been measured. This in turn is an extension of the work described by de Heer and Van den Bos[29]). These cross sections are given in table IX.
In the case of excitation the n^1P measurements are pressure dependent due to absorption of resonance n^1P–1^1S radiation and have been omitted therefore. However, for a correct calculation of the cascade to n^1S the pressure-dependent n^1P data have been used. For He^+ on He, a separate measurement at 60° (see section 3.2) of capture and excitation was possible only down to

TABLE I

Investigated transitions in helium

transition	λ (Å)	transition	λ (Å)
3^1S–2^1P	7281	3^3S–2^3P	7065
4^1S–2^1P	5048	4^3S–2^3P	4713
5^1S–2^1P	4438	5^2S–2^3P	4121
3^1P–2^1S	5016	3^3P–2^3S	3889
4^1P–2^1S	3965	4^3P–2^3S	3188
		5^3P–2^3S	2945
3^1D–2^1P	6678	3^3D–2^3P	5876
4^1D–2^1P	4922	4^3D–2^3P	4472
5^1D–2^1P	4388	5^3D–2^3P	4026
		6^3D–2^3P	3820

about 3 keV. Below this energy the two processes were measured simultaneously. The sum of the experimental capture and excitation cross sections are given in table X only at those energies, where the separation could not be performed. These cross sections do not contain a lifetime correction for the unknown part of the cross section determined by the capture process. At small impact energies, this correction is relatively small but not negligible for those levels with a relatively long lifetime.

As we stated before (section 3.1) each cross-section curve was determined in three energy regions with different ion accelerators. The differences among the cross sections in the overlapping energy regions give an indication about the reproducibility of the results. The mean relative deviations found are listed in table XI. In order to obtain a continuous energy dependence of the cross section, the three parts of the cross-section curves were fitted together by taking the average of the cross sections in the overlapping areas and multiplying the other cross sections with corresponding scaling factors.

The reproducibility is connected to random errors in the measurement of the beam current (1%), the photomultiplier current (2%), the gas pressure (2%) and the intensity calibration (5%). In the case of small cross sections, or small light signals owing to the use of small slit widths in the case of close neighbour spectral lines, the random error in the photomultiplier current may be larger.

The main systematic error arises from the absolute calibration of the Leiss monochromator. For the calibration with the tungsten standard lamp it is dependent on the wavelength and extends between 5 and 9% for the 6256S-type photomultiplier (for a more detailed discussion see sections 3.5 and 5.1 of ref. 12). For 3^1S, 3^1D and 3^3S cross sections, which were obtained from measurements with the 9558B-type photomultiplier, additional systematic errors of about 20% may be present (see ref. 12). Other systematic errors may occur in the current measurements of the ion beam and the light intensity (2%), in the determination of the geometrical quantities ω and L (2%) and in the McLeod calibration (3%).

In order to check some of these systematic errors we remeasured cross sections for the 4^1S excitation of helium in the case of protons incident on helium. This reaction was chosen because the measurement is relatively simple; the cross section is derived from the 4^1S–2^1P transition (5047 Å), with no polarization and very small cascade effects. Further many previous measurements and theoretical calculations have been carried out for this process. In table XII we compare our data with previous measurements of our group[11,12]). In general the agreement is reasonable. By analysing the data of our group together with those of other experiments and theory (see refs. 12, 30, 31, 32 and 33) we estimate that the absolute values of this work in table XII are within about 20% consistent with theory.

In the case of electron-capture measurements two additional systematic

TABLE II

$\sigma_{capture}$ in 10^{-20} cm^2 for He$^+$ on He

E (keV)	3^1S	4^1S	5^1S	3^1P	4^1P	3^1D	4^1D	5^1D	3^3S	4^3S	5^3S	3^3P	4^3P	5^3P	3^3D	4^3D	5^3D	6^3D
1.0							7.31	2.78				20.8	3.06		133	28.6		
1.5							10.3	3.74		4.00		20.2	1.87		114	36.7		
2.0							5.04	2.35		2.11		21.1	1.62		118	23.5	10.9	
2.5		0.88					3.67	1.96		2.22		30.0	4.50		98.5	20.2	6.46	
3.0		1.14		23.5			4.34	1.43		3.56		24.1	3.24		88.3	16.4	5.00	
3.5		1.74		29.4			6.04	1.91		3.07		34.2	2.80		89.1	20.5	7.14	
4		1.31		33.7	8.72		7.84	1.90		3.10		38.1	2.68		94.4	24.6	8.59	
5		1.19		28.5	4.86		7.98	2.12		3.20	1.20	32.9	3.64	1.30	128	29.8	9.52	3.87
6		1.55		31.7	7.15		8.03	2.86		4.07		50.5	6.56		133	17.8	9.93	
7		2.36		43.1	7.25		6.89	2.83	26.4	4.43	1.08	76.8	4.86	1.49	98.5	11.9	10.6	4.23
8		3.90		69.1	6.22	53.8	8.25	2.34	28.1	5.89		81.2	5.84		69.8	14.5	6.06	
9		4.45		87.6	7.06	50.5	10.5	1.99	30.2	6.29		75.2	8.24		66.5	16.3	7.23	
10	21.8	3.87		80.3	11.0	49.4	12.0	3.66	30.0	7.88	1.52	64.0	11.0	2.05	66.3	14.8	8.6	2.22
12.5	17.7	3.01		69.5	15.2	51.6	6.34	5.30	24.6	5.82	0.74	64.7	10.0	3.51	80.5	11.7	7.86	4.00
15	19.3	3.60	3.15	57.1	16.3	75.1	7.34	4.07	24.8	6.41	1.59	67.5	9.0	3.80	84.9	13.7	7.46	2.95
17.5	23.6	3.97	2.08	52.0	15.0	85.7	12.0	3.86	27.0	6.69	2.58	71.0	7.56	4.52	85.8	19.0	8.75	2.16
20	25.4	4.58	2.16	49.9	15.1	94.6	15.1	4.55	29.0	8.44	2.02	70.2	7.90	4.40	78.1	20.4	10.0	3.92
22.5	25.1	4.82	3.48	49.2	15.3	107	18.3	6.09	30.8	9.45	2.20	69.8	9.0	4.67	68.3	20.1	9.60	5.15
25	25.0	4.98	3.32	48.3	15.8	111	22.1	7.13	33.0	10.2	3.63	67.4	9.5	5.06	72.2	23.2	10.3	5.17
27.5	27.2	5.30	3.69	46.3	17.1	106	23.6	8.07	35.0	9.89	3.50	71.2	10.5	4.53	79.3	25.5	11.2	6.48
30	30.3	6.10	3.96	47.2	18.6	97.2	22.2	9.47	36.0	11.0	3.84	70.8	11.2	8.53	95.5	28.8	11.7	6.28
35	39.5	6.52	4.23	51.6	20.1	93.0	23.7	11.6	39.0	12.4	3.90	74.0	11.9	8.07	109	33.5	14.2	7.20
40	51.2	7.76	4.61	61.4	31.0	82.8	26.7	13.5	49.9	15.1	5.11	82.9	12.9	6.21	96.0	33.5	14.5	6.47
50	74.9	13.1	5.73	104	39.4	64.7	31.2	14.7	87.6	20.6	7.33	94.7	17.9	8.53	78.2	29.4	15.3	6.77
60	85.3	16.8	8.48	127	46.2	62.9	34.1	18.3	145	27.7	9.92	105	21.2	10.4	64.1	26.4	13.2	6.46
70	99.9	22.3	11.3	139	56.3	55.1	32.5	17.6	165	29.2	13.6	110	22.5	11.4	47.5	21.5	12.1	6.37
80	116	24.3	11.9	145	63.0	47.2	27.9	16.6	187	45.3	16.2	115	24.8	12.4	41.6	16.6	9.82	4.05
90	107	25.0	12.1	142	60.7	36.2	23.9	13.7	280	55.2	23.4	87.6	21.6	13.1	34.7	15.2	9.32	4.66
100	129	22.8	12.7	136	52.8	34.9	18.5	11.4	306	66.4	27.9	112	29.6	13.2	29.0	13.3	7.61	4.08
110	139	23.6	11.9	125	56.5	30.7	11.2	6.63	329	80.2	34.2	122	33.9	14.3	22.6	11.4	4.82	4.35
120	133	23.7	10.2	122	49.9	25.4	8.65	5.59	334	82.5	38.1	126	36.9	15.1	21.2	10.4	3.59	3.33
130	130	22.8	10.7	114	49.0	24.0	7.92	4.81	343	88.9	41.8	133	38.6	15.6	22.2	8.97	3.07	
140	143	22.4		99.0	47.0	15.6	6.12	4.48	352	84.7	40.9	128	40.1	13.8	20.5	8.08	2.62	
150	138	22.0		86.8	37.6	14.1	4.17	3.57	384	84.3	42.3	131	40.5	15.3	16.3	6.60	2.15	

TABLE III

$\sigma_{capture}$ in 10^{-20} cm^2 for He$^+$ on Ne

E (keV)	3^1S	4^1S	5^1S	3^1P	4^1P	3^1D	4^1D	5^1D	3^3S	4^3S	5^3S	3^3P	4^3P	5^3P	3^3D	4^3D	5^3D	6^3D
0.3		1.56		83.2			21.9				2.73	77.5	9.0	3.40	245	59.2	10.3	
0.5		2.68		174		526	35.0		185	13.0	3.57	60.1	17.3	4.64	352	56.2	18.0	
0.7		5.28		152	34.0	515	37.7		158	13.0	3.26	100	10.2	4.32	382	61.6	21.9	
1.0		8.94		154	45.5	521	37.3		121	12.3	2.84	137	14.3	5.39	394	74.9	17.4	
1.5		8.46		240	26.4	427	61.7		101	11.2	2.39	156	15.0	7.73	557	96.6	19.1	
2.0	23.2	8.93		220	32.7	481	53.8		101	14.7	3.03	117	16.2	9.58	605	79.5	23.2	
2.5	34.9	4.76		226	38.7	481	36.5		121	11.5	2.40	135	22.1	9.50	576	67.8	16.9	
3.0	49.0	8.10		205	37.1	478	34.2		133	11.2	2.37	161	29.9	8.88	567	79.5	17.5	
3.5	42.5	14.4		195	34.7	496	43.9		129	13.1	2.76	169	30.3	9.34	568	85.0	22.1	
4	51.0	13.2	13.2	173	26.0	497	53.4		113	13.6	2.69	161	27.5	14.1	565	96.6	27.2	
5	61.1	8.60		114	21.2	458	55.1	9.17	113	12.1	7.13	136	27.1	14.9	490	88.4	21.4	6.83
6	65.8	9.34		102	20.4	437	43.3		101	11.9	8.60	140	29.7	13.3	426	62.1	22.7	
7	53.8	10.4		118	23.1	414	34.5	12.4	90.8	13.3	9.20	174	30.9	13.9	370	48.3	21.5	8.97
8	42.4	19.5		153	31.9	398	29.8		87.3	16.2	8.08	201	33.1	14.8	327	42.0	17.5	
9	51.9	24.9		189	33.5	373	30.7		93.7	20.0	5.89	217	34.1	15.5	294	42.2	14.2	
10	71.4	24.8		193	39.5	350	37.3	11.0	110	23.3	5.64	228	33.5	15.2	289	43.2	14.1	7.73
12.5	135	14.2		161	47.2	282	46.3	11.1	189	20.3	4.73	146	30.7	14.3	280	46.1	16.1	7.70
15	148	18.8		85.1	50.9	282	37.3	16.3	214	21.3	5.23	104	35.1	13.8	277	43.2	18.3	9.11
17.5	133	30.9		66.3	44.2	284	33.0	14.8	206	27.1	5.64	87.2	35.1	16.3	268	35.5	17.6	10.8
20	101	40.2		73.4	37.0	285	37.3	11.2	180	35.0	6.43	88.2	33.0	18.6	255	34.8	15.5	10.6
22.5	85.6	41.8		80.7	30.7	275	44.0	10.2	166	39.8	8.29	99.1	30.0	16.5	248	36.0	13.8	9.28
25	66.5	37.1		92.5	25.8	261	52.4	11.9	159	41.2	10.6	109	28.6	15.4	235	40.5	15.2	9.59
27.5	59.1	31.6		113	25.6	243	37.4	16.3	157	40.5	13.0	120	30.0	13.4	235	45.1	17.4	10.2
30	57.4	24.9		121	33.0	234	58.2	18.9	174	39.5	14.4	143	37.4	14.6	233	50.0	21.3	11.1
35	67.8	18.2		198	42.6	219	61.2	22.4	190	40.4	13.9	204	50.2	20.3	213	56.6	30.0	13.7
40	77.0	18.8		174	46.1	213	62.9	23.6	207	45.2	15.3	237	59.7	23.5	200	61.4	35.5	16.5
50	165	22.7		174	53.7	172	56.5	18.2	317	65.0	19.1	280	75.5	32.7	182	69.4	41.0	19.3
60	204	34.6		154	45.9	138	46.9	17.5	433	93.1	28.7	308	87.4	43.5	156	72.8	43.4	20.7
70	193	40.1		151	43.3	111	42.2	14.4	536	125	41.5	348	99.6	51.2	125	69.9	45.3	22.6
80	181	43.9		149	43.0	94.1	36.8	10.9	578	151	58.1	371	109	55.0	103	62.0	45.7	22.0
90	178	42.1		119	49.3	78.4	32.0	10.7	615	162	65.7	394	115	57.2	88.3	53.6	40.7	20.5
100	184	42.7		99.9	42.0	69.7	26.9	9.68	633	153	68.9	433	116	56.6	77.5	48.3	33.2	18.3
110	168	38.6		91.9	37.5	51.8	23.2	7.78	581	135	71.3	380	116	52.9	69.3	42.3	28.8	14.4
120	185	34.2		91.4	32.9	45.4	18.8	6.41	573	126	65.6	345	103	48.7	60.0	34.5	24.4	13.1
130	169	31.5		103	28.0	38.7	16.7	5.29	513	118	64.0	319	108	43.7	49.6	34.0	21.2	11.9
140	162	32.7		87.0	25.9	34.3	14.1	4.81	493	110	62.8	299	104	41.4	40.8	29.8	18.7	10.2
150	158	31.2		74.9	22.6	29.8	12.3	4.33	443	107	61.5	277	101	40.2	36.9	26.3	16.3	

TABLE IV

$\sigma_{capture}$ in 10^{-20} cm^2 for He$^+$ on Ar

E (keV)	3^1S	4^1S	5^1S	3^1P	4^1P	3^1D	4^1D	5^1D	3^3S	4^3S	5^3S	3^3P	4^3P	5^3P	3^3D	4^3D	5^3D	6^3D
0.3		2.07					8.71					47.9	6.77		160	18.6		
0.5		3.54				233	7.89					56.7	7.03		139	10.5	5.30	
0.7		3.65				264	11.4			5.51		78.9	7.07		126	27.5	4.84	
1.0		5.96				296	20.8		157	15.3		90.3	16.3		151	34.6	4.85	
1.5		8.56				284	27.2		154	22.8		124	16.2		208	49.9	12.9	
2.0		7.14				322	26.9		226	18.5		154	18.1		285	43.6	11.8	
2.5		6.10				395	27.2		251	15.6		180	23.9		383	54.2	14.5	
3.0		9.84				465	33.9		221	21.8		223	28.0		440	63.8	18.8	
3.5		14.4				465	36.2		238	25.2		272	30.6		473	69.4	21.5	
4		18.9				488	41.0		248	28.9		322	33.2		519	72.8	26.7	
5		20.4				474	40.3	8.26	288	41.1		401	42.0		548	80.9	26.1	9.3
6	42.7	19.1				375	37.4		333	51.2		396	44.5		552	80.5	24.3	
7	50.8	21.4				352	43.0	8.72	305	41.2		311	42.6		557	82.2	25.4	12.8
8	57.1	25.5				387	40.7		281	37.6		366	43.1		533	81.9	28.6	
9	62.9	29.6				382	44.9		261	36.5		386	44.7		515	83.7	31.8	
10	58.7	28.2				370	46.7	13.1	248	35.8	15.3	355	43.6		498	83.9	31.2	12.8
12.5	63.7	16.0				318	49.0	14.5	240	33.6	13.1	311	39.7		383	79.4	31.5	14.2
15	59.4	12.9				293	49.8	15.1	251	31.3	12.0	300	42.9		365	76.8	32.4	15.6
17.5	55.7	15.2				276	51.4	16.8	249	32.3	12.7	291	49.6		353	75.4	34.2	17.2
20	53.4	17.3				285	52.5	18.3	265	36.8	14.1	290	52.3		369	78.2	36.8	18.6
22.5	54.4	19.9				307	58.5	19.2	297	42.3	16.3	298	57.2		399	94.3	39.5	20.2
25	58.0	20.8				329	54.6	19.6	328	47.4	18.7	312	62.7		418	95.8	43.1	21.9
27.5	51.7	22.8				333	58.1	19.9	378	53.1	21.6	330	70.3		452	105	46.2	24.2
30	70.5	26.7				340	60.0	23.3	459	59.2	24.8	356	86.7		454	111	50.5	29.9
35	93.4	36.6				345	68.6	32.3	694	77.3	32.3	438	130		458	127	57.3	39.8
40	113	44.5				354	77.6	33.6	851	122	48.7	515	154		489	157	68.1	50.4
50	180	63.4				325	86.3	39.8	1292	232	103	697	198		513	192	86.4	66.4
60	259	78.8				261	89.1	41.8	1529	333	139	881	231		489	197	98.2	73.4
70	310	89.9				241	86.8	36.9	1643	394	160	1032	261		428	176	98.8	79.8
80	338	96.9				216	82.7	35.1	1657	414	167	1115	281		400	158	87.9	70.5
90	324	98.7				217	72.7	31.0	1632	392	176	1145	294		349	142	81.1	70.9
100	302	97.6				183	63.3	32.1	1565	352	172	1120	300		313	130	75.2	59.2
110	301	94.1				162	55.5	27.6	1454	357	171	1137	292		242	113	71.3	54.5
120	267	87.9				133	47.7	23.9	1478	301	162	1123	278		186	98.0	61.9	52.3
130	260	86.7				118	43.3	22.1	1367	276	145	1081	275		162	82.4	52.8	46.1
140	245	83.8				105	39.2	20.3	1287	253	139	1013	273		140	69.5	46.8	42.8
150	248	77.5				95.9	36.7	16.8	1207	234	125	977	269		121	60.4	42.7	39.0

TABLE V

$\sigma_{capture}$ in 10^{-20} cm^2 for He$^+$ on Kr

E (keV)	3^1S	4^1S	5^1S	3^1P	4^1P	3^1D	4^1D	5^1D	3^3S	4^3S	5^3S	3^3P	4^3P	5^3P	3^3D	4^3D	5^3D	6^3D
0.3							18.1					4.11			27.1			
0.5							17.2					7.16	0.72		42.8			
0.7							15.6					14.4	1.48		53.8			
1.0		19.3				96.7	16.4		31.3	5.65		34.5	4.02		113	22.7		
1.5		18.6				146	16.4		60.7	8.09		52.5	6.42		187	37.7		
2.0		19.1				182	21.8		89.9	10.6		73.2	11.0		250	46.7	11.3	
2.5		23.4				243	25.9		95.4	13.6		97.2	14.8		309	52.0	12.7	
3.0	65.5	25.5		106		269	28.1		105	16.4		123	18.0		354	57.5	14.5	
3.5	67.2	26.8		113		332	32.6		112	18.8		161	21.0		385	60.9	15.6	
4	68.2	27.2		117		409	37.2		104	20.6		179	23.8		399	61.2	17.1	
5	50.4	23.5		95.3		376	41.3	6.55	100	22.9	4.32	191	29.1	15.9	463	71.5	20.6	6.2
6	58.6	24.4		95.4		283	31.6		114	23.5		198	40.3		437	74.1	24.0	
7	56.9	25.5		127		243	34.2	9.82	126	24.9	5.56	220	45.4	18.7	449	79.7	26.1	11.1
8	64.1	26.4		147		232	46.0		133	31.0		255	53.7		469	85.6	33.5	
9	68.1	30.5		138		261	52.7		134	39.3		293	59.0		488	91.7	36.5	
10	71.7	32.7		170		253	52.1	13.8	148	32.2	6.08	330	68.2	15.9	498	98.9	39.1	13.4
12.5	107	31.1		257		241	48.6	18.4	171	33.2	7.41	358	74.6	18.8	521	104	40.6	16.1
15	117	35.0		285		254	51.3	26.9	142	37.4	9.37	389	94.9	21.4	533	107	40.1	18.8
17.5	124	35.2		297		295	54.5	34.3	202	43.1	13.7	390	112	26.4	563	117	45.1	21.3
20	125	36.8		310		335	57.7	39.0	260	49.3	16.5	402	126	33.0	615	130	49.4	24.0
22.5	136	38.5		320		375	61.3	39.2	298	52.0	18.3	420	145	36.4	677	150	53.1	26.4
25	148	39.8		334		394	68.1	38.1	397	55.8	19.6	431	166	43.9	693	172	57.2	28.7
27.5	150	41.2		347		411	76.5	43.4	482	67.9	19.8	444	185	54.5	716	188	62.7	30.7
30	157	41.8		419	114	417	84.7	46.9	617	76.5	19.8	484	197	63.2	735	209	76.4	38.2
35	213	53.0		532	154	416	100	47.0	1008	116	34.9	546	233	94.3	808	258	91.7	60.6
40	269	66.8		553	108	413	119	55.2	1310	189	53.5	639	263	118	868	292	115	73.0
50	429	106		623	149	431	136	59.7	1846	374	159	849	315	133	950	349	153	84.0
60	520	144		637	186	449	129	54.7	2054	526	240	1109	361	158	907	365	168	97.6
70	596	172		665	227	395	120		2141	608	299	1328	404	176	751	334	173	101
80	589	189		775	246	363	112		2062	649	323	1469	441	168	643		161	98.4
90	595	196		704	267	342	106		1922	651	316	1558	470	181	574		145	86.1
100	593	184		746	285	305	100		1778	533	290	1575	482	188	494		131	84.3
110	443	190		822	236	281	85.1		1667	463	270	1439	492	171	442		117	71.0
120	420	190		753	247	248	74.7		1510	411	248	1333	466	181	353		108	63.7
130	406	178		763	226	206	68.6		1504	396	228	1288	485	170	309		101	60.1
140	387	171		745	209	174	63.2		1362	375	212	1253	483	171	283		92.3	56.3
150	402	159		684	208	144	60.2		1289	357	205	1233	489	174	244		86.9	52.3

TABLE VI

$\sigma_{capture}$ in 10^{-20} cm^2 for He^+ on Xe

E (keV)	3^1S	4^1S	5^1S	3^1P	4^1P	3^1D	4^1D	5^1D	3^3S	4^3S	5^3S	3^3P	4^3P	5^3P	3^3D	4^3D	5^3D	6^3D
0.3												15.6	5.90		116	72.6		
0.5						265						19.3	7.41		137	82.1		
0.7						170						21.3	7.07		158	89 1		
1.0						166				112		19.2	8.37		194	96.4		
1.5						199			190	118		30.6	11.7		262	106		
2.0						294			166	130		46.9	16.2		327	106		3.71
2.5						281			152	140		79.7	19.6		343	113		4.91
3.0						290	36.0		152	143		87.3	23.9		379	119		6.53
3.5						346	46.0		166	135		118	24.7		409	117		7.66
4	72.6					329	49.8		176	131		114	26.7		447	113	44.3	9.79
5	81.5					335	45.2		173	117	3.94	130	29.9		479	108	44.8	8.48
6	92.9			147		319	52.1		185	113		183	35.7		523	114	51.6	9.97
7	82.6			166		323	67.9	6.69	197	106	12.9	285	45.8		581	116	66.8	
8	97.4	24.7		213		341	84.9		227	111		334	57.8		611	128	77.7	
9	90.4	32.5		237		357	85.1		248	112		412	64.6		610	140	83.2	
10	88.8	40.5		285		334	76.4	16.7	221	99.9	13.3	432	73,5		590	145	86.0	17.3
12.5	129			344		332	39.6	22.2	241	93.6	15.3	453	95.6		740	152	88.1	24.5
15	137			366		462	41.0	24.3	307	104	25.5	483	125		882	160	89.0	29.3
17.5	156	29.9		370		489	48.2	28.8	394	114	32.8	521	157		1041	174	94.1	31.6
20	183	44.8		383		559	55.0	33.7	542	124	37.8	567	123		1220	208	102	33.4
22.5	213	51.1		401		617	66.7	40.0	718	137	39.3	615	150		1330	250	115	38.6
25	241	57.2		415		657	79.4	43.0	944	151	39.3	684	181		1420	297	128	46.3
27.5	265	63.5		445		675	89.0	49.0	1205	173	40.5	811	212		1514	347	142	56.5
30	292	69.1		467		657	96.4	62.2	1498	212	48.1	886	232		1614	387	154	75.3
35	375	98.2		554		676	141	82.7	2107	336	68.8	955	273		1694	454	177	110
40	520	137		541		634	192	93.7	2674	438	118	1304	335		1752	509	189	130
50	567	187		687		582	297	113	3246	679	255	1850	491		1772	578	222	152
60	561	224		665		554	327	116	3431	860	378	2276	590		1669	618	244	161
70	641	247		831		511	324	127	3261	947	464	2484	650		1505	621	251	161
80	585	270		789		481	280	124	2764	984	490	2585	689		1337	522	225	159
90	629	286		692		431	225		2577	968	489	2668	712		1175	429	211	151
100	545	287		699		373	190		2598	895	445	2726	725		1026	385	203	141
110	565	268		642		343	167		2445	840	392	2587	735		878	341	186	125
120	528	245		622		301	139		2312	778	348	2432	743		763	312	170	111
130	482	236		620		268	128		1669	711	330	2316	726		662	275	158	97.0
140	447	226		571		244	106		1500	649	313	2151	707		575	235	151	88.0
150	409	208		512		200	89.4		1202	618	297	2052	666		507	203	145	80.8

TABLE VII

Polarization $I_{///}/I_{\perp}$ of emission lines induced by electron capture in the case of

	He+ on He					He+on Ne			He+ on Ne/de Heer *et al.*[1])	
E (keV)	3^1P–2^1S	4^1D–2^1P	4^3P–2^3S	3^3D–2^3P	3^1P–2^1S	4^1D–2^1P	4^3P–2^3S	3^2D–2^3P	3^1P–2^1S	4^1D–2^1P
0.3	0.72	0.80	0.78	0.93				1.20		
0.5	1.29	0.66	0.82	0.98	1.77	1.00	0.93	1.08		
0.7	1.32	0.78	0.84	0.97				1.10		
1.0	1.20	0.98	0.88	1.04	0.94	1.09	0.92	1.08		
1.5	1.40	0.75	0.82	1.02				1.00		
2.0	1.63	0.94	0.79	1.06	0.80		0.96	1.02		
2.5	1.60	1.30	0.82					1.10		
3.0	1.35	1.12	0.77	1.15	0.66	0.90	0.86	1.13		
3.5	1.36		0.72							
4	1.35	1.05	0.74	1.20	0.92	0.88	0.94	1.16		
5	1.44		0.73		0.90	0.92	0.93	1.17	0.97	0.93
6	0.92	1.40	0.62	1.20		1.12	0.94			
7			0.68		0.75			1.17	0.70	
8	1.05	1.47	0.75		0.85	1.30				1.36
9			0.65							
10	0.893	1.78	0.66	1.22	1.30	1.50	0.94	1.12	1.37	1.34
12.5									1.88	1.88
15			0.90		1.72	1.67	0.96	1.01	1.79	2.06
17.5									1.50	
20		1.81	0.89		1.47	1.68	0.97	1.10	1.48	1.70
22.5					1.55					
25	1.09	1.81	0.91	1.45	1.70	1.65	0.96	1.14	1.77	1.76
27.5										
30	1.51	2.09	0.91	1.39	1.84	1.66	1.09	1.06	1.86	1.76
35	1.44	2.09	0.91	1.42	1.71		1.10	1.15	1.76	1.77
40	1.29	2.12	0.93	1.50	1.50		1.20	1.20		
50	0.93	2.28	1.00		1.37	2.00	1.23	1.24		
60	0.99	2.06	1.03	1.41	1.10	2.07	1.13	1.31		
70	1.13				0.92	1.87	1.13	1.41		
80		1.99	1.18	1.30	1.05	1.81	1.03	1.45		
90					1.08	1.88	1.09	1.39		
100	1.46	2.06	1.26	1.28	1.14	1.90	1.11	1.42		
110					1.19	1.98	1.09	1.43		
120	1.60	1.80	1.14	1.20	1.22	2.00	1.08	1.33		
130					1.30	2.16	1.10	1.23		
140	1.60	1.70	1.06	1.18	1.42	1.94	1.16	1.22		
150	1.75	1.96	1.04	1.13	1.45	2.03	1.10	1.13		

TABLE VIII

Polarization $I_{//}/I_{\perp}$ of emission lines induced by electron capture in the case of

	He+ on Ar			He+ on Kr		He+ on Xe		
E (keV)	4^1D–2^1P	4^3P–2^3S	3^3D–2^3P	3^1P–2^1S	4^1D–2^1P	4^3P–2^3S	3^3D–2^3P	4^1D–2^1P	4^3P–2^3S	3^3D–2^3P
0.3										0.96
0.5	0.94		0.86			1.10				
0.7										
1.0	0.98	1.08	1.06		0.85	1.04	1.05			0.98
1.5										
2.0	0.93	0.93	1.09	1.32	0.94	0.97	1.11			1.01
2.5										
3.0	1.07			1.45	0.83	1.02	1.15			1.12
3.5										
4	1.15	0.98	1.13	1.39	1.03		1.21			1.22
5	1.07				1.12	0.94	1.24	1.32		1.24
6	0.93	0.98	1.16	1.27						
7					1.11					
8	1.20									
9										
10	1.50	1.01	1.04		1.31	1.03	1.24	1.31	0.96	1.24
12.5			1.10							
15	1.66	0.96	1.07		1.53	1.03	1.23	1.53	1.05	1.23
17.5										
20	1.38	0.97	1.08		1.57	1.11	1.34	1.27	1.14	1.34
22.5										
25	1.50	0.99	1.14		1.51	1.17	1.37	1.11	1.13	1.37
27.5					1.58					
30	1.50	1.01	1.16		1.45	1.09	1.33	1.55	1.04	1.33
35	1.63					1.05	1.31	1.42	0.99	1.31
40	2.00	1.00	1.30		1.30		1.30	1.30	1.02	
50	1.98	1.02	1.31		1.21	1.05	1.31	1.34	1.10	1.25
60	1.95	1.06	1.34		1.40	1.08	1.32	1.40	1.13	1.23
70	1.90	1.08	1.40		1.45	1.12	1.42	1.36	1.19	1.24
80	1.82	1.11	1.18		1.55	1.14	1.40	1.29	1.24	1.24
90	1.80	1.11	1.20		1.48	1.16	1.30	1.29	1.28	1.24
100	1.78	1.11	1.22		1.41	1.17	1.29	1.24	1.30	1.23
110	1.75	1.16	1.27		1.37	1.18	1.17	1.24	1.32	1.20
120	1.73	1.21	1.35		1.38	1.20	1.22	1.17	1.38	1.16
130	1.60	1.21	1.31		1.36	1.22	1.27	1.15	1.40	1.15
140	1.57	1.21	1.27		1.34	1.23	1.16	1.12		1.15
150	1.50	1.21	1.30		1.18	1.25	1.11	1.11	1.39	1.15

TABLE IX

$\sigma_{excitation}$ in 10^{-20} cm²

E (keV)	3^1S	4^1S	5^1S	3^1D	4^1D	5^1D	3^3S	4^3S
1.0					8.28	1.99		
1.5					9.45	2.78		3.75
2.0		0.72			6.13	1.92		2.34
2.5		0.67			5.93	1.95		2.46
3.0		0.91			6.00	1.52		3.49
3.5		1.23			6.69	1.41		3.46
4.0		1.47			7.30	1.44		3.01
5.0		1.54			6.46	1.67		3.71
6.0		1.42			6.27	2.42		5.08
7.0		2.05			8.06	2.06		6.10
8.0		2.82			8.31	2.05		5.12
9.0		4.17			11.3	2.56		5.32
10.0		4.96		40.8	13.2	3.42	62.4	6.72
12.5	29.3	4.55		54.4	15.0	6.90	58.9	11.0
15.0	28.1	4.33	2.56	71.9	11.5	7.34	62.6	11.1
17.5	33.8	5.07	3.06	92.3	12.7	5.30	76.2	8.68
20.0	37.7	6.30	3.37	102	20.1	4.41	85.6	6.70
22.5	37.7	6.50	3.51	104	28.8	5.80	93.3	6.57
25.0	39.9	6.75	3.58	103	36.2	8.59	102	7.48
27.5	40.7	6.80	3.58	102	42.7	11.5	110	9.52
30.0	40.6	7.00	3.68	103	44.2	13.5	98.3	11.0
35		9.18			44.4	15.6		13.1
40		10.4			39.6	11.9		16.2
50		12.2	4.80		27.4	11.0		19.5
60		11.8	4.38		19.2	8.64		24.2
70		9.90	4.38		13.8	6.08		28.8
80		8.80	3.95		11.2	4.94		28.5
90		8.81	4.04		10.8	4.75		23.6
100		9.30	4.76		9.60	4.47		25.3
110			4.67		8.47	3.81		24.0
120			5.53		8.42	4.00		21.9
130			6.43		9.79	4.72		21.1
140			7.09		11.3	5.28		19.4
150			8.08		11.3	5.23		19.1

for He^+ on He

5^3S	3^3P	4^3P	5^3P	3^3D	4^3D	5^3D	6^3D
	20.7	2.19		150	29.9		
	19.7	2.28		123	35.0	10.9	
	29.9	1.94		140	26.6	10.4	
	29.0	3.31		145	16.6	8.23	
	34.1	2.86		124	18.5	5.75	
	29.2	2.19		107	20.3	5.95	
	19.6	2.00		97.4	20.7	6.15	
	31.9	2.75		88.7	18.4	5.81	
	43.2	3.42		83.6	15.9	6.22	
2.94	42.5	2.80		91.9	15.5	7.61	
	45.2	3.98		98.7	14.6	7.37	
	53.0	5.65		93.2	15.1	7.78	
2.72	60.7	6.17	5.00	84.6	17.3	7.80	2.60
3.39	62.2	8.81	6.56	80.4	18.6	8.12	3.10
4.53	59.9	10.6	8.67	96.8	17.0	7.97	4.42
5.11	51.3	10.9	8.58	122	18.6	6.95	4.47
4.86	53.2	10.6	8.84	142	25.9	7.09	3.25
4.04	60.0	10.4	7.81	160	35.0	10.2	3.08
2.82	72.6	10.9	6.79	151	39.5	12.4	4.13
2.86	79.1	11.3	6.85	141	41.7	14.8	4.78
2.83	83.0	12.7	6.69	127	41.8	16.2	6.50
3.98	102	17.6	8.34	116	37.3	17.2	7.42
4.65	114	16.6	8.42	101	33.2	16.2	8.18
5.59	116	22.5	12.4	77.0	25.8	15.3	8.01
7.44	117	28.3	13.1	58.4	22.3	13.2	7.02
8.46	102	24.9	13.7	44.3	17.9	11.3	6.03
7.85	97.9	21.7	13.5	42.6	14.4		5.20
9.32	62.3	15.4	12.9	33.8	12.6		4.54
8.81	70.4	15.8	12.0	27.3	10.4		3.87
8.13	68.5	14.0	9.85	19.9	9.52		2.73
7.78	59.1	17.5	9.68	16.1	8.96		2.73
7.77	45.2	16.9	9.08	17.1	6.17		2.51
7.05	51.2	15.6	8.03	16.2	6.21		2.41
6.89	50.9	14.5	7.23	13.6	5.18		2.06

TABLE X

$\sigma_{\text{excitation+capture}}$ in 10^{-20} cm^2 for He^+ on He

(at impact energies where capture and excitation were observed together)

E (keV)	4^1S	4^1D	5^1D	3^3S	4^3S
0.3	2.13	20.1	6.28		1.98
0.5	1.83	18.8	4.85		1.97
0.7	1.41	17.4	6.29	53.2	2.77
1.0	2.53			40.2	3.53
1.5	2.23			46.2	

E (keV)	3^3P	4^3P	3^3D	4^3D	5^3D
0.3	36.5	6.56	360	89.2	23.2
0.5	25.7	6.03	303	71.1	19.7
0.7	32.6	6.37	289	74.2	25.0
1.0					12.2
1.5					21.7

E (keV)	3^1S	3^3S
2	38.2	40.4
4	33.4	37.4
6	40.6	49.4
8	41.6	

TABLE XI

The mean relative deviations in our experimental cross sections in the overlapping energy regions of the three accelerators

	He^+ on He (%)	He^+ on Ne (%)	He^+ on Ar (%)	He^+ on Kr (%)	He^+ on Xe (%)
3^1S	25	20	7	7	19
4^1S	18	13	18	23	15
5^1S	20				
3^1P	28	22		16	17
4^1P	25	13		27	
3^1D	8	10	8	5	20
4^1D	23	11	9	11	15
5^1D	24	29	8	15	9
3^3S	20	15	4	22	3
4^3S	25	20	10	13	19
5^3S	20	18	15	9	15
3^3P	17	11	13	10	12
4^3P	26	17	13	12	11
5^3P		11		23	
3^3D	16	20	19	10	14
4^3D	15	15	15	5	8
5^3D	12	14	12	15	9
6^3D	10	29	30	5	11

TABLE XII

4^1S excitation cross sections for protons on helium (units 10^{-20} cm^2)

E (keV)	This work	Van den Bos *et al.*[12])	Van Eck *et al.* (revised)[12, 11])
20	27.8	20.6	24.8
30	47.7	40.8	46.5
50	56.0	47.1	48.9
70	49.2	45.1	43.7
100	39.1	35.1	38.2
150	27.3	22.1	

errors may be present: we have remarked that some lifetimes used in the lifetime correction (see section 6) might not be accurate. The worst case is 4^3P with an uncertainty of 12% leading to a possible error in the cross section of at most 10% at 150 keV. The error due to the slit correction procedure (see section 9.2) is estimated to be smaller than 5%.

Another error is present in the $5\,^3D$ cross section, because the $5\,^3D$–$2\,^3P$ radiation is contaminated with that of $7\,^1S$–$2\,^1P$. In the case of electron capture the effect is estimated to be smaller than 3%. In the case of excitation (see table IX) the contamination increases with impact energy and may give a contribution of about 14% to $\sigma(5\,^3D)$ at 80 keV. In our estimation we have assumed that $\sigma \propto n^{-3}$ and taken into account the lifetime correction (section 6) in the case of electron capture.

In the polarization measurements random errors are present in the determination of $I_{//}$ and $I_{\perp}$. The random error in this ratio is about 5%, except in the case of very weak signals when the corresponding cross sections are small. Systematic errors due to stray magnetic fields in our collision chamber are small (see ref. 12).

12. *Comparison with other experiments.* Previous work on capture of electrons into excited states in collisions of He^+ on He has been reported by our group[3, 1]) between 7.5 and 90 keV. The present experiment must be seen as an extension of this work with various improvements in experimental procedure. The absolute calibration has been carried out more accurately (section 4). The accelerator between 30 and 150 keV provided larger and more stable He^+ currents than in the previous experiment. In the previous work no correction had been made for Doppler broadening of spectral lines, the lifetime correction has been studied here also more carefully by using different geometrical conditions (variation of length l, see section 9.1). Our present results should therefore be more reliable than those of ref. 3. As far as He^+ on He is concerned, comparison can also be made with measurements of Head and Hughes[2]) between 20 and 120 keV.

TABLE XIII

Comparison between capture cross sections of the present and previous work of our group[3]) and of Head and Hughes[2]) for He^+ on He (units 10^{-20} cm^2)

	4^1S			3^1P			4^1D		
E (keV)	Present	Previous	Head, Hughes	Present	Previous	Head, Hughes	Present	Previous	Head, Hughes
30	6.1	5.04	11	47.2	50.1	170	22.2	16.5	28
60	16.8	15.6	45	127	112	215	34.1	21.9	42.5
90	25.0	19.0	59	142	140	275	23.9	15.3	37
120	23.7		65	122		220	8.65		22.5
	4^3S			3^3P			4^3D		
30	11.0	6.18	23	70.8	48.6	127	28.8	17.2	38
60	27.7	17.6	69	105	70.7	185	26.4	13.5	37
90	55.2	41.2	140	87.6	76.6	235	15.2	7.56	23.3
120	82.5		203	126		270	10.4		

TABLE XIV

Comparison between capture cross sections of the present work and those of ref. 1 for He^+ on Ne (units 10^{-20} cm^2)

	4^1S		4^1D		3^1P	
E (keV)	Present	Ref. 1	Present	Ref. 1	Present	Ref. 1
5	8.60	11.5	55.1	63	114	150
7.5	15	11.8	32	52	136	158
10	24.8	20.8	37.3	29	193	283
12.5	14.2	14.6	46.3	47	161	260
15	18.8	12.2	37.3	45	85.1	175
17.5	30.9	21.7	33.0	33.8	66.3	130
20	40.2	32.5	37.3	36.2	73.4	231
22.5	41.8	36.2			80.7	141
25	37.1	38.0	52.4	44	92.5	189
30	24.9	27.3	58.2	56	121	245
35	18.2	18.3	61.2	57	198	258

In table XIII we present some of our present and previous results and those of Head and Hughes.

Differences are found both in the absolute values and the energy dependence of the cross sections. As far as absolute values are concerned the difference between our present results and those of Head and Hughes is similar to those found in investigations for excitation of helium by protons. In that case the 4^1S cross sections of Dodd and Hughes[34]) are about 2 times larger than ours and probably too large[12]) (see also section 11).

In table XIV we compare our present cross sections for He^+ on Ne with those of de Heer *et al.*[1]). For 4^1S and 4^1D the agreement is generally reason-

able, for 3^1P the cross sections differ by a factor of about two above 10 keV. In ref. 1 cross sections have also been obtained for He(3^1P) formation in the case of He^+ on He and He^+ on Kr by observation of 3^1P–1^1S radiation of He at 537 Å. These cross sections between 5 and 35 keV are generally in bad agreement with the present data and less accurate.

As far as the energy dependence is concerned careful experiments have been made by Dworetsky *et al.*[5]) for He^+ on He and by Tolk *et al.*[6]) for He^+ incident on Ne, using ion beams with good energy resolution ($\approx$ 1 eV) between threshold and 5 keV. These experiments show more detailed structure in the cross section energy curves than in our case. The meaning of this structure is discussed in section 14.

For He^+ incident on argon and xenon, no other optical measurements are known to us to compare with our present results.

For completeness we remark that for the symmetrical combination He^+, He the present excitation cross sections in table IX are probably more accurate than those in ref. 29. Some data are compared in table XV.

TABLE XV

Comparison between excitation cross sections of the present and of previous work of our group[29]) for He^+ on He (units 10^{-20} cm^2)

E	4^1S		4^1D		4^3S		4^3P		4^3D	
(keV)	present	previous	present	previous	present	previous	present	previous	present	previous
20	6.30	3.96	20.1	10.1	6.70	3.19	10.6	4.47	25.9	16.0
40	10.4	7.83	39.6	29.0	16.2	8.22	16.6	6.01	33.2	26.4
60	11.8	8.81	19.2	13.0	24.2	11.5	28.3	9.44	22.3	17.9
80	8.80	6.93	11.2	7.69	28.5	12.5	21.7	8.65	14.4	11.6

Measurements on polarization of radiation for He^+ on Ne can be compared with measurements of de Heer *et al.*[1]) (see table VII). The agreement is generally good. For He^+ on He the data between 25 and 55 keV were taken from ref. 3 and not remeasured.

13. *General discussion of results.* In figs. 10 to 14 we illustrate some of our results in graphs. In almost every curve a most pronounced peak is present between about 30 and 150 keV. The location of such a peak is often correlated with the adiabatic criterion of Massey[35]). On the basis of semi-classical arguments Massey predicts one maximum or resonance in the cross section located approximately at an impact energy such that the product of the effective collision time τ multiplied by the frequency ν of the electronic excitation transition is unity or

$$\tau \cdot \nu = \frac{a}{v} \frac{\Delta E}{h} \approx 1. \qquad (26)$$

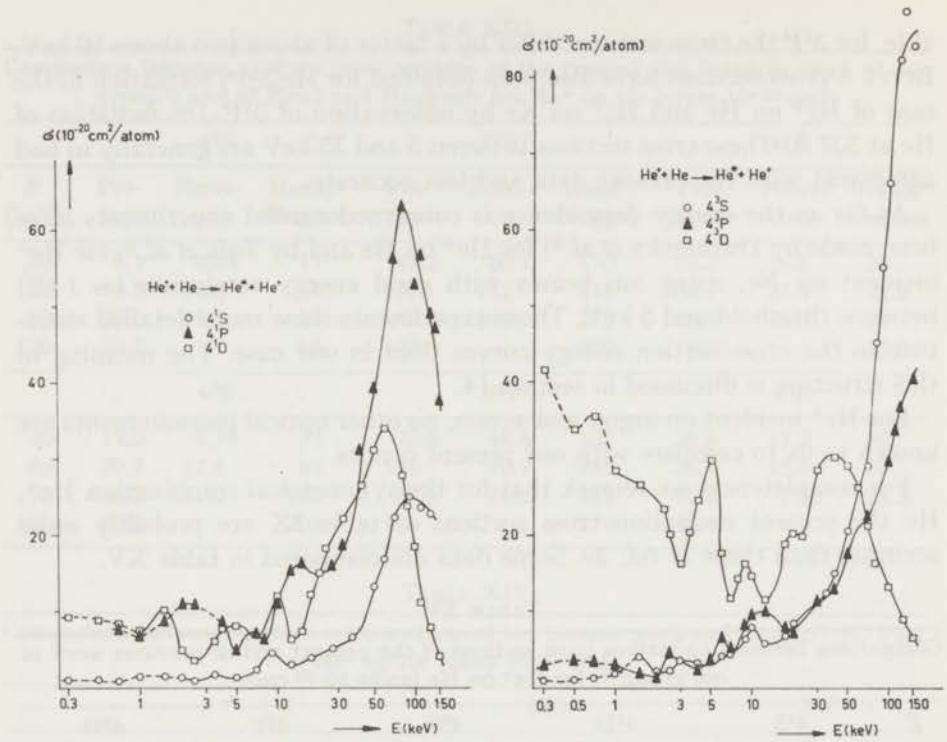

Fig. 10. Cross sections for electron capture into singlet and triplet S, P and D states in the case of He^+ on He.

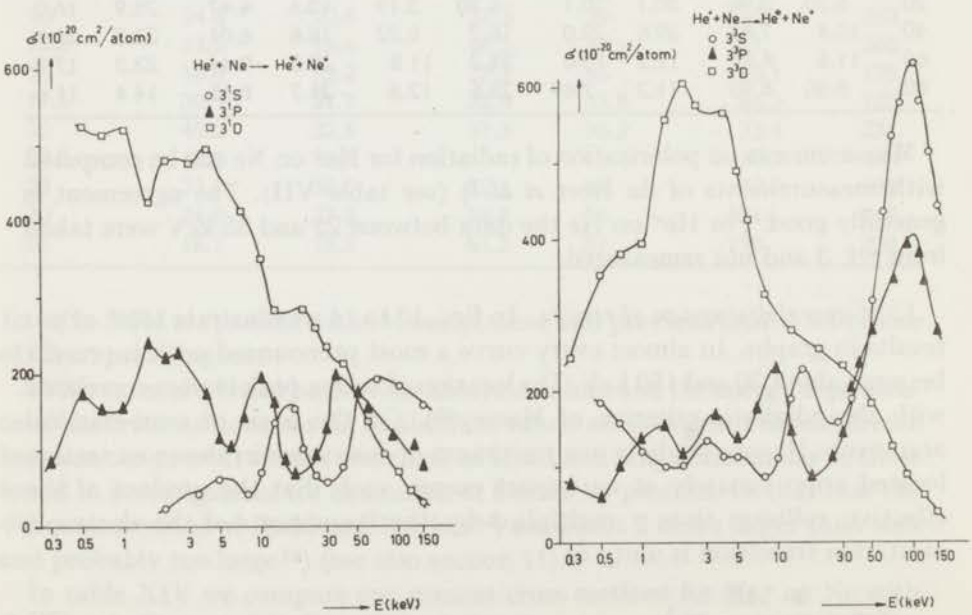

Fig. 11. Cross sections for electron capture into singlet and triplet S, P and D states in the case of He^+ on Ne.

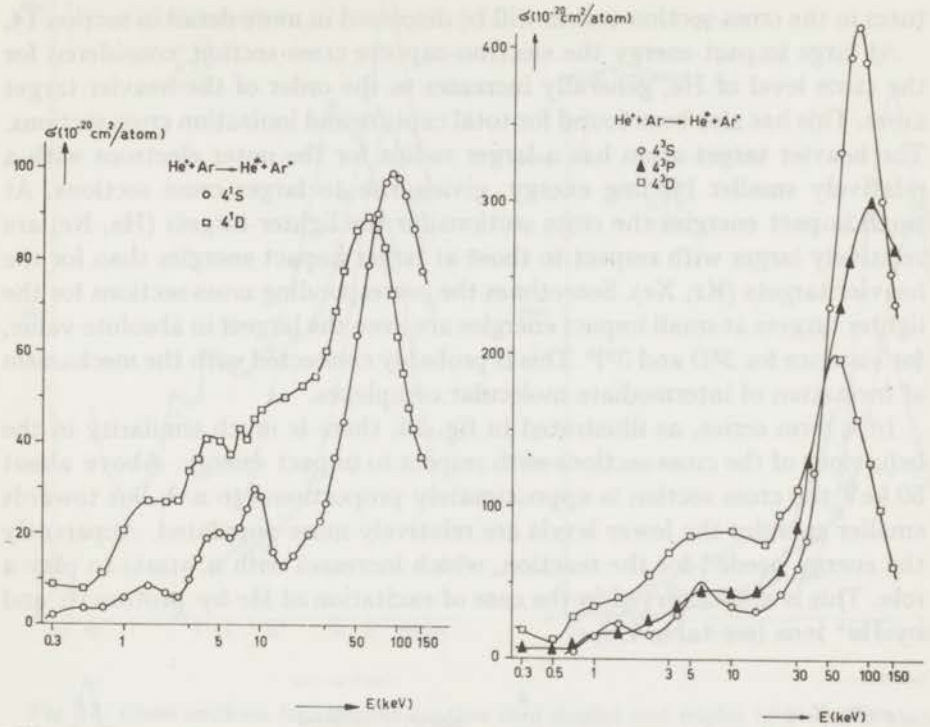

Fig. 12. Cross sections for electron capture into singlet and triplet S, P and D states in the case of He^+ on Ar.

Here v is the velocity of the projectile at the maximum, a is the effective interaction distance, h is Planck's constant and ΔE is the change of potential energy for the collision products before and after the collision. In our capture reactions ΔE varies from about 22 eV in the case of He^+ on He to 10 eV in the case of He^+ on Xe. By application of eq. (26) we find that the locations of the main peaks in figs. 10 to 14 correspond to a values varying between 3 and 7 Å. This is of the same order of magnitude as found for other capture, ionization and excitation processes (see for instance Hasted[36]), Solov'ev *et al.*[37]) and Van den Bos *et al.*[12])).

Besides the main peak in our cross-section curves (see figs. 10–14) many peaks or oscillations are found at smaller impact energies. This behaviour cannot be explained with the simple adiabatic criterion of Massey. It is connected with the formation of an intermediate molecular complex, possibly with pseudo crossing of potential curves (see for instance Dworetsky *et al.*[5])). This mechanism gives rise to a smaller effective value of $a \cdot \Delta E$ than that used in Massey's criterion where only the initial and final atomic states of the collision products are taken into account. From eq. (26) it is then clear that the smaller $a \cdot \Delta E$ value gives rise to peaks in the cross section at relatively smaller impact velocities as affirmed experimentally. The struc-

tures in the cross-section curves will be discussed in more detail in section 14.

At large impact energy the electron-capture cross section, considered for the same level of He, generally increases in the order of the heavier target atom. This has also been found for total capture and ionization cross sections. The heavier target atom has a larger radius for the outer electrons with a relatively smaller binding energy, giving rise to larger cross sections. At small impact energies the cross sections for the lighter targets (He, Ne) are relatively larger with respect to those at larger impact energies than for the heavier targets (Kr, Xe). Sometimes the corresponding cross sections for the lighter targets at small impact energies are even the largest in absolute value, for instance for 3^3D and 3^3P. This is probably connected with the mechanism of formation of intermediate molecular complexes.

In a term series, as illustrated in fig. 15, there is much similarity in the behaviour of the cross sections with respect to impact energy. Above about 50 keV the cross section is approximately proportional to n^{-3}, but towards smaller energies the lower levels are relatively more populated. Apparently the energy needed for the reaction, which increases with n, starts to play a role. This is also observed in the case of excitation of He by protons[12]) and by He^+ ions (see table IX).

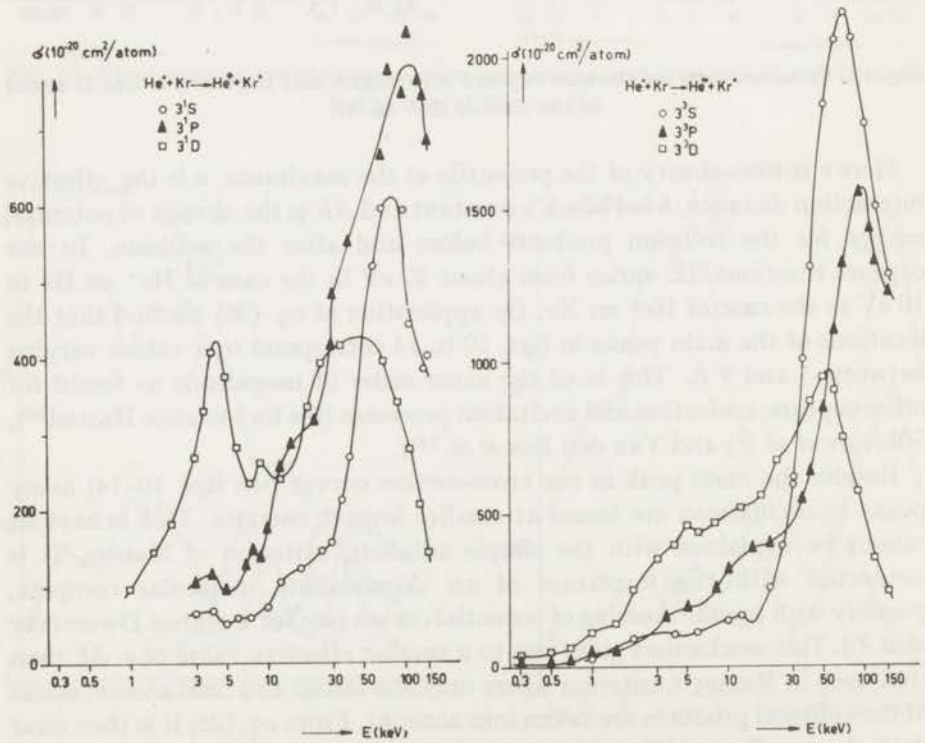

Fig. 13. Cross sections for electron capture into singlet and triplet S, P and D states in the case of He^+ on Kr.

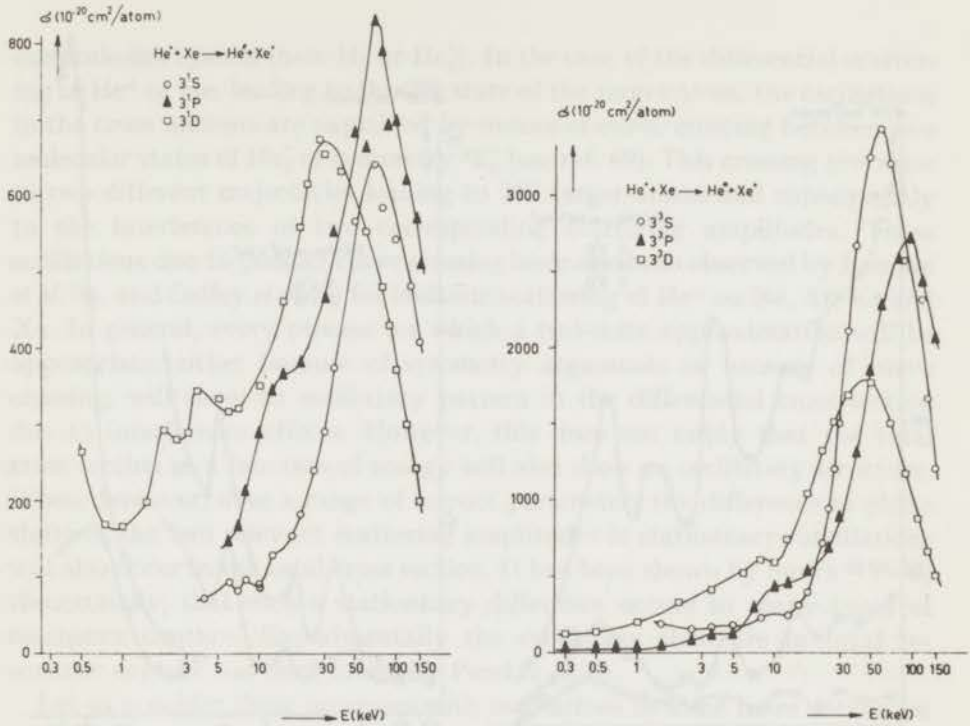

Fig. 14. Cross sections for electron capture into singlet and triplet S, P and D states in the case of He^+ on Xe.

It is often found that the structure in the cross-section curves is similar for a singlet and triplet level of He with the same n, l quantum numbers, except at the smaller impact energies. This is shown for He^+ on He in fig. 16. For the S levels and often for the P and D levels the triplet cross sections are larger than the corresponding singlet cross sections (same n value) in a large energy region; the difference is about a factor three for the S levels which is the same as the difference in statistical weight.

At our larger impact energies, the cross section is the smallest for D cross sections with respect to S and P levels, all compared for equal n; for the latter two levels there is no clear systematics in their relative size. It may be that somewhere above 150 keV the S cross sections become larger than the P cross sections just as found for electron capture into excited states for H^+ on He and Ne by Pretzer *et al.*[38]) and Jaecks *et al.*[39]). In theoretical calculations[40,41]) for H^+ on H it is found that the capture cross section decreases in order of S, P and D levels at large impact energy, as partly confirmed by our and the other mentioned experiments. At small impact energies, the order is often reverse (see figs. 10–14). The relative strong size of the D cross sections at these energies may be connected to the relative importance of large momentum transfer and the formation of levels with higher azimuthal quantum number (see also ref. 10).

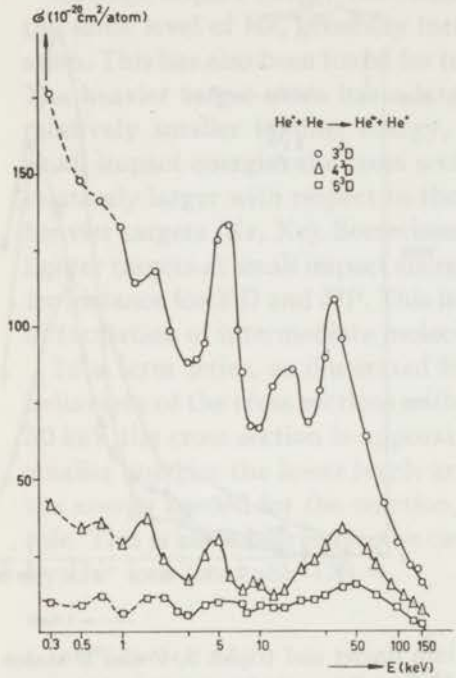

Fig. 15. Cross sections for electron capture into triplet D states in the case of He^+ on Xe.

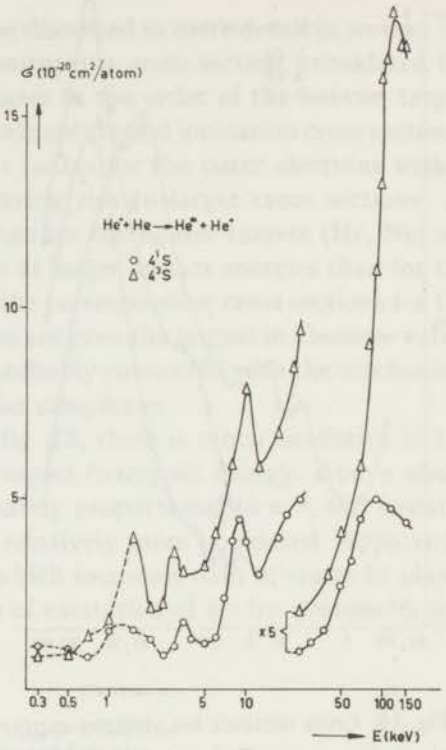

Fig. 16. Cross sections for electron capture into the 4^1S and 4^3S states in the case of He^+ on He.

Much structure is found in the polarization of radiation as a function of energy in those cases where the cross section also exhibits structure. However there is not always a clear correlation between these structures in the cross section and polarization.

14. *Discussion of the oscillatory structure in the cross sections.* In most cases the description for the experimentally observed oscillations in differential and total elastic and inelastic cross sections has been given in terms of a two-state approximation, treating the paths of the heavy particles classically (see for instance refs. 42, 43, 44, 45, 46). A clear distinction should be made between differential and total cross sections.

Let us first consider differential scattering. Experiments for H^+ on H[45]) and for He^+ on He[47, 48]) have shown regular oscillations in cross sections for elastic scattering and resonance-capture scattering as a function of angle at a fixed impact energy and reverse. These oscillations are due to an interference of the scattering amplitudes $f_g(\theta)$ and $f_u(\theta)$, which depend on the gerade and ungerade potentials, $V_g(r)$ and $V_u(r)$, of the intermediate

molecule-ion system (here H_2^+ or He_2^+). In the case of the differential scattering of He^+ or He, leading to the 2^3S state of the target atom, the oscillations in the cross sections are explained by means of curve crossing between two molecular states of He_2^+ of symmetry $^2\Sigma_g^+$ (see ref. 49). This crossing gives rise to two different trajectories leading to 2^3S target atoms and consequently to the interference of two corresponding scattering amplitudes. These oscillations due to (single) curve crossing have also been observed by Baudon *et al.*[50]), and Coffey *et al.*[51]) for inelastic scattering of He^+ on Ne, Ar, Kr and Xe. In general, every process for which a two-state approximation will be appropriate, either because of symmetry arguments or because of curve crossing, will show an oscillatory pattern in the differential cross section due to interference effects. However, this does not imply that the total cross section as a function of energy will also show an oscillatory structure. When, however, over a range of impact parameters the difference in phase shifts of the two relevant scattering amplitudes is stationnary, oscillations will also occur in the total cross section. It has been shown by Smith[46 52, 53]) theoretically, that such a stationnary difference occurs in many cases of resonance capture. Experimentally the oscillating structure in total resonance capture has been found by Perel *et al.*[54]).

Let us consider these processes with oscillations in some more details for H^+ on H and look at a fixed angle to the probability of resonance capture scattering as a function of impact energy. Then oscillations will occur at succeeding velocities v_n and v_{n+1} for which the difference between the phase shifts η_u and η_g varies with 2π.

Here η_u and η_g are the phase shifts in the ungerade (via the $2p\sigma_u$ state of H_2^+) and in the gerade (via the $1s\sigma$ state of H_2^+) scattering. The following equations have been derived (see for instance refs. 43 and 44):

$$\phi = \eta_u - \eta_g \simeq \frac{1}{\hbar v} \int_{-\infty}^{\infty} [\varepsilon_u(R) - \varepsilon_g(R)]\, dR \tag{27}$$

and

$$\frac{1}{v_n} - \frac{1}{v_{n+1}} \simeq \left[\frac{1}{\hbar} \int_{-\infty}^{\infty} [\varepsilon_u(R) - \varepsilon_g(R)]\, dR\right]^{-1}. \tag{28}$$

For simplification of notation, further on, we shall use the symbols

$$\Delta 1/v_n = 1/v_n - 1/v_{n+1}, \tag{29}$$

$$\langle a \Delta E \rangle = \int_{-\infty}^{\infty} [\varepsilon_u(R) - \varepsilon_g(R)]\, dR, \tag{30}$$

so that

$$\Delta 1/v_n = h/\langle a \Delta E \rangle. \tag{31}$$

As we have noticed before, the oscillations occur also in the total cross section for resonance capture as a function of impact velocity or energy. In a two-state approximation this cross section can be presented by[46]:

$$\sigma = 2\pi \int_0^\infty b \sin^2(\eta_u - \eta_g)\, db, \tag{32}$$

where b is an impact parameter and $\eta_u - \eta_g$ the phase difference as defined in eq. (27). Oscillations in total cross sections are connected with a stationary phase difference, which occurs when $\varepsilon_u(R) - \varepsilon_g(R)$ passes through a maximum. As Smith has pointed out[46,52,53] such a maximum occurs at relatively large internuclear distance as a consequence of a minimum in the potential of the binding state of the intermediate molecular ion and at relative small internuclear distance corresponding to "core" scattering. In a similar way one can predict oscillations in cross sections of elastic or inelastic non-resonance processes where pseudo crossing of potential curves occurs [43,49,50,51].

Another type of oscillations has been measured by Dworetsky *et al.*[4,5] in the case of He^+ on He in the total cross section for formation of excited He-atoms by excitation and electron capture together. These oscillations are explained by Rosenthal and Foley[55]. They are caused by an interference of two outgoing inelastic channels at such a large internuclear separation that this type of oscillation is not expected to be present in the corresponding

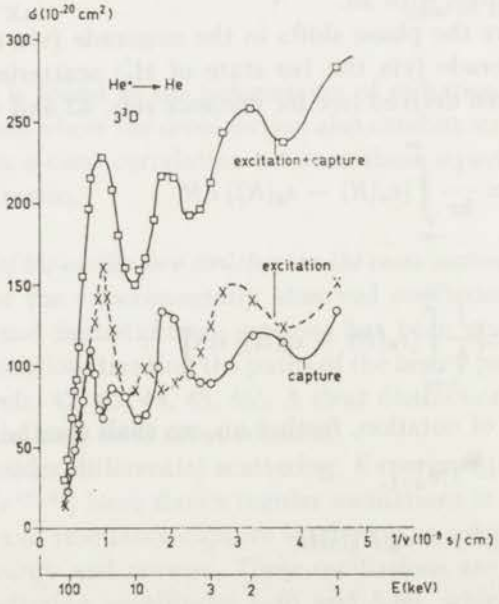

Fig. 17. Excitation and capture cross sections for 3^3D formation as a function of the inverse velocity in the case of He^+ on He.

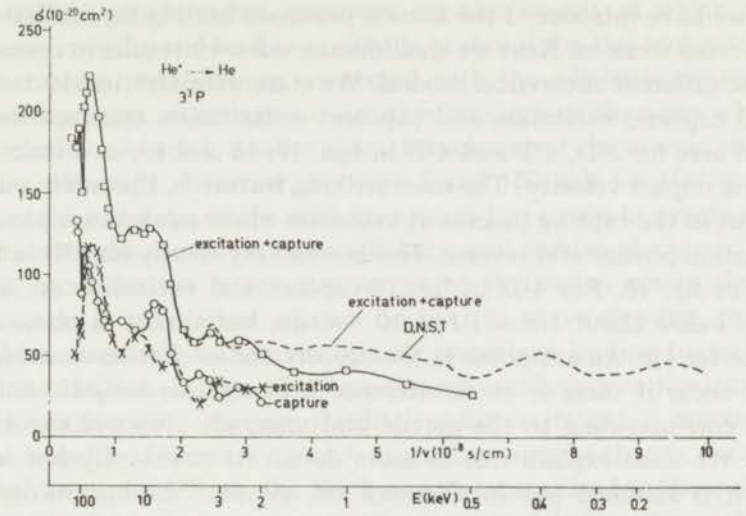

Fig. 18. Excitation and capture cross sections for 3^3P formation as a function of the inverse velocity in the case of He^+ on He. *D*, *N*, *S*, *T* corresponds to ref. 4.

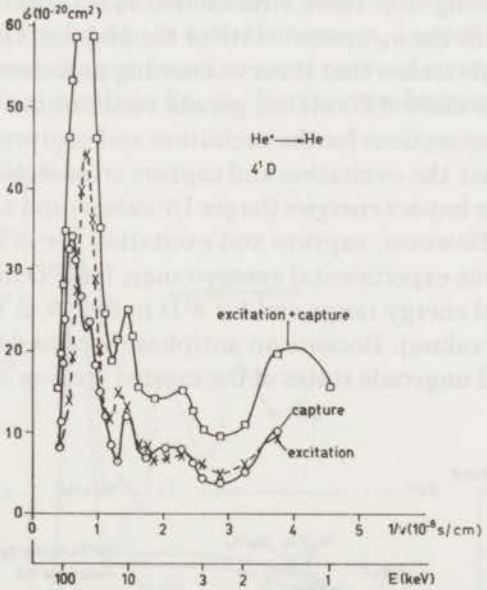

Fig. 19. Excitation and capture cross sections for 4^1D formation as a function of the inverse velocity in the case of He^+ on He.

differential cross section as a function of angle. The oscillations are seen for instance in the cross sections for formation of 3^1S and 3^3S states, with a phase difference so that the maxima for 3^1S are obtained at the same velocity as the minima for 3^3S and reverse.

So far we have introduced the known processes leading to oscillations in the total cross sections. Next we shall discuss our own results in connection with these different theoretical models. We start with He^+ incident on He. Our total capture, excitation and capture + excitation cross sections are presented here for 3^3D, 3^3P and 4^1D in figs. 17, 18 and 19, as a function of the inverse impact velocity. The most striking feature is, that often maxima are present in the capture process at velocities where minima are present in the excitation process and reverse. This is seen very clearly for 3^3D in fig. 17 and 3^3P in fig. 18. For 4^1D in fig. 19 capture and excitation are also in antiphase below about $1/v = 1.7 \times 10^{-8}$ s/cm., but almost in phase above that value for $1/v$. An antiphase in the capture and excitation cross sections can only occur if there is an interference between two inelastic outgoing channels corresponding to the gerade and ungerade states of the excited He_2^+ ion. We shall explain this in more detail. At sufficiently low impact energies it is assumed (see for instance ref. 49) that the intermediate excited states of the He_2^+ ion in the collision process are chiefly formed by curve crossing and that this curve crossing only occurs for gerade states of the He_2^+ ion. This is schematically shown in the level scheme of He_2^+ taken from Lichten[44]) (see fig. 20). There is no excited σ_u state of the He_2^+ ion having a curve crossing with the σ_u ground state of the He_2^+ ion, the latter being the lowest σ_u state. This means that if curve-crossing processes are important in the formation of the excited He states, gerade states of the He_2^+ play a role, leading to equal cross sections for the excitation and capture process. For 4^1D we see in fig. 19 that the excitation and capture cross sections come close together at the smaller impact energies (larger $1/v$ values) and are almost in phase at those energies. However, capture and excitation are in antiphase for 3^3P in fig. 18 in our whole experimental energy range, for 3^3D in fig. 17 over most of our experimental energy range and for 4^1D in fig. 19 at the higher impact energies (lower $1/v$ values). Because an antiphase is caused by an interference between gerade and ungerade states of the excited He_2^+ ion and curve crossing

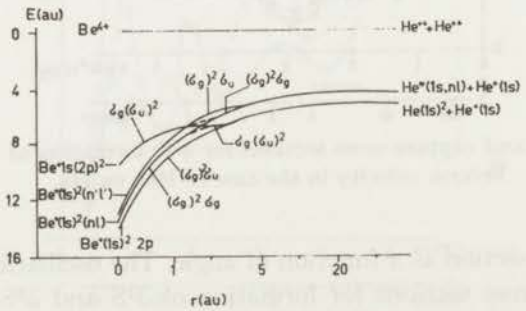

Fig. 20. Level scheme of He_2^+ (see refs. 48, 57 and 58).

only occurs via gerade states, processes are also important which do not go via curve crossing and lead to excited σ_u states of the He_2^+ molecule ion.

Curve crossing processes are connected with the adiabatic character of the collision process, dominating over other reaction mechanisms when the impact velocity v is much smaller than the velocity of the atomic electrons $v_0 = 2.2 \times 10^8$ cm/s). However, between 5 and 150 keV for He^+ on He, v becomes of the order v_0 and the collision process just comes in a region where the reaction mechanism is no more adiabatic and sudden electronic transitions can occur (in the latter case we go to the region where the Born approximation is valid when $v \gg v_0$). So next to curve crossing, processes with sudden electronic transitions become important leading to excited σ_u states of the He_2^+ ion. In figs. 17–19 we also see oscillations in the total cross sections for excitation + capture. Oscillations for excitation + capture have also been found by Dworetsky *et al.*[4]) at smaller energies than in our experiments; in the case of 3^3P (see fig. 18) their data (normalized on those of ref. 3) are given in a limited energy range. As mentioned before, Rosenthal and Foley[55]) explained the oscillations of Dworetsky *et al.*[4]) by an effect of curve crossing at large nuclear separation. We think that many of our oscillations are due to another effect: their oscillations show for instance an anti-phase between singlet and triplet levels with the same n, l quantum numbers (see ref. 55), which is generally not found in most parts of our energy range. This is illustrated for 4^1D and 4^3D in fig. 21. Further the frequency of their oscil-

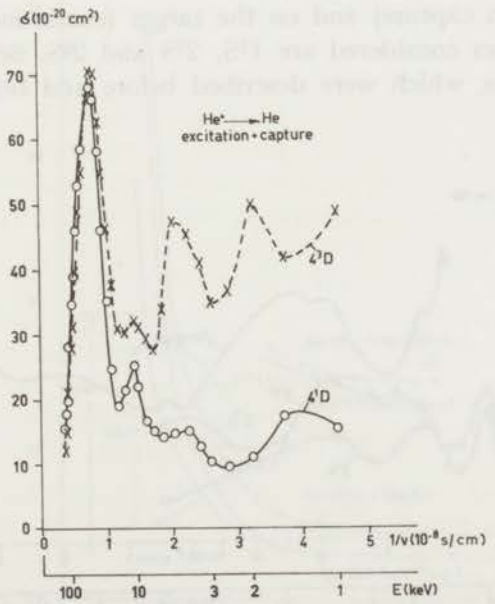

Fig. 21. Cross sections for excitation + capture of 4^1D and 4^3D as a function of the inverse velocity in the case of He^+ on He.

lations is often smaller than in our experiment. For instance for He 3^3P (see fig. 18) we find that our average value of $\Delta 1/v$ is about 9.3×10^{-9} s cm^{-1} or $\langle a\Delta E\rangle = 43$ eV Å (see eq. 31), while in the case of Dworetsky *et al.*[4]) an analysis of Tolk and White (private communication) gives

$$\Delta 1/v_n \simeq 2.5 \times 10^{-8} \text{ s cm}^{-1} \quad \text{or} \quad \langle a\Delta E\rangle = 16 \text{ eV Å}.$$

The relevant oscillations of Dworetsky *et al.*[4]) have such a frequency that at energies above 5 keV only one or no oscillations are expected, different from our results. In the case of He 4^3S a few oscillations near 2 keV are present in the experiment of Dworetsky *et al.*[4]) which have a frequency close to that in our experiment:

$$(\Delta 1/v_n \simeq 1.1 \times 10^{-8} \text{ s cm}^{-1} \quad \text{and} \quad \langle a\Delta E\rangle \simeq 37 \times 10^{-8} \text{ eV cm}).$$

Our oscillations in excitation + capture might be due to curve crossing of the gerade He_2^+ ground state and a gerade He_2^+ excited state (see fig. 20) at relatively small nuclear separation, explaining also the earlier found structure in differential scattering leading to 2^3S excitation[49]). This would mean that not only in resonance capture but also is nonresonance reactions with curve crossing oscillations are found both in differential and total cross sections.

Theoretical calculations for He^+ on He have been performed by Sural *et al.*[56]) for total cross sections of 2^1S and 2^3S formation both by excitation and electron capture between 0.6 and 40 keV. They used an impact-parameter treatment in which the coupling between excited atomic states on the projectile (electron capture) and on the target (excitation) is taken into account. The states considered are 1^1S, 2^1S and 2^3S. So the mentioned interference effects, which were described before and believed to be re-

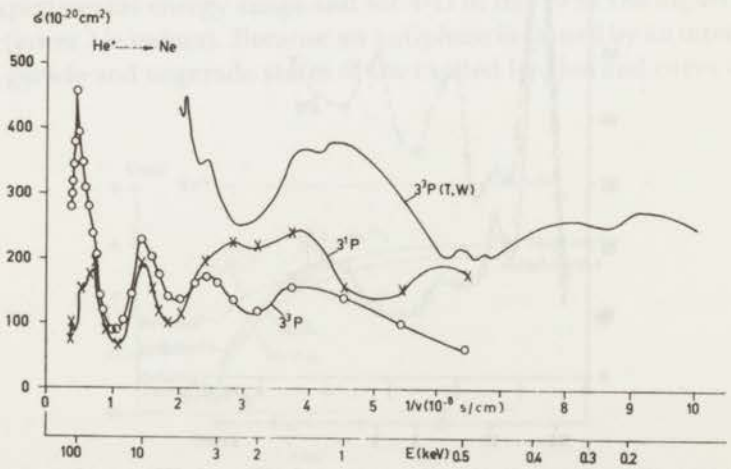

Fig. 22. Capture cross sections for 3^1P and 3^3P formation as a function of the inverse velocity in the case of He^+ on Ne. *T*, *W* corresponds to ref. 6.

sponsible for the antiphase in the capture and excitation cross sections in the experiment, should also be found in the theoretical calculations. However, in most of the energy range (0.6–40 keV) Sural *et al.*[56]) find that both for 2^1S and 2^3S the theoretical excitation and capture cross sections are almost equal to each other and no sharp structure as found in the experiment is present.

Wilets and Gallaher[57]) have carried out similar coupled-state calculations for H^+ on H considering 1S, 2S, $2P_0$ and $2P_{\pm1}$ states both on the projectile and the target. Although total cross sections for 2S are not in phase for excitation and capture, the theoretical results do not bear a clear relation with the phenomena observed in the total cross sections in He^+, He experiments. In fig. 22 we show our data for He^+ on Ne, where the 3^1P and 3^3P capture cross sections are plotted versus $1/v$. Included are also the data of Tolk and White[6]) who have measured relative cross sections as a function of impact energy and normalized their cross sections by using data of ref. 3 for the same excited He level. Tolk and White have explained the oscillations in the cross sections by means of potential curve crossing, making use of the calculations of Michels[58]) for the lowest energy levels of the $(Ne\ He)^+$ system. The curves are presented in fig. 23. The incoming channel corresponds to $B^2\Sigma$ when $He^+(^2S_{\frac{1}{2}})$ collides with $Ne(^1S_0)$. The final state, $He(3^3P) + Ne^+(^2P_{\frac{1}{2}})$

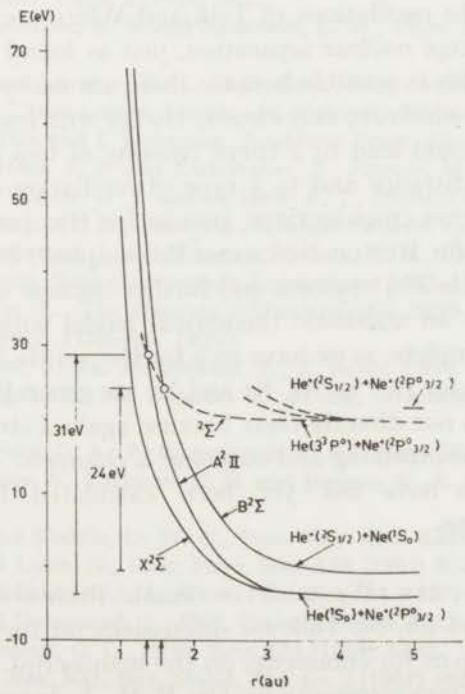

Fig. 23. Energy level diagram of the $(He\ Ne)^+$ moleculear complex (see refs. 58 and 6).

can be populated by Σ, Π and Δ outgoing molecular channels. The positions of the two crossing points with the Σ outgoing channel have been introduced by Tolk and White, making use of the experimental thresholds for He (3^3P) formation both when He^+ is incident on Ne and when Ne^+ is incident on He. Lichten [59]) has shown that pseudo curve crossing can also occur between molecular states with different Λ numbers, taking into account the correlation of electrons. Probably at relatively small impact energies the interaction between the incoming and outgoing Σ channels is the strongest, being responsible for oscillations in elastic and inelastic scattering experiments and probably also for those in the total capture cross sections as found in our experiment and by Tolk and White [6]). However, the frequency of the oscillations in our experiment is much higher than in that of Tolk and White. For He 3^3P formation (see fig. 22) we have in our case

$$\Delta \frac{1}{v_n} \simeq 1 \times 10^{-8} \text{ s cm}^{-1} \quad \text{or} \quad \langle a\Delta E \rangle \simeq 41 \text{ eV Å},$$

while an analysis of Tolk and White (private communication) gives in their case

$$\Delta \frac{1}{v_n} \simeq 4.4 \times 10^{-8} \text{ s cm}^{-1} \quad \text{or} \quad \langle a\Delta E \rangle \simeq 9.4 \text{ eV Å}.$$

It might be that the oscillations of Tolk and White are connected with a curve crossing at large nuclear separation, just as found for He^+ on He as discussed before. This is possible because there are many outgoing channels of $He^+(^2S_{\frac{1}{2}}) + Ne^*$, which are very close in energy with respect to $He(3^3P) + Ne^+(^2P_{\frac{3}{2}})$. This could lead to a curve crossing of two outgoing channels at relatively large distance and to a type of oscillation only seen in total capture and excitation cross sections, just as for He^+ incident on He. The explanations given for He^+ on Ne cannot be complete, because little is yet known about the $(He\ Ne)^+$ system and further because our data are in an energy region were an adiabatic theoretical model with a two-state approximation is incomplete, as we have seen for He^+ on He. Oscillations found in our cross sections for He^+ on Ar, Kr and Xe are generally less pronounced than for Ne. This is not directly clear because again a strong interaction is expected between the incoming and outgoing Σ channels. To our knowledge molecular diagrams have not yet been calculated for the He^+–Ar, –Kr and –Xe systems.

Acknowledgements. We wish to thank Professor J. Kistemaker, Professor J. Los and Dr. N. Tolk for discussions on the experimental results and Dr. L. Vriens for comments on the manuscript. We are indebted to assistance in the measurements by Drs R H J. Janssen, Drs. B. F. J.

Luyken and Mrs. R. W. Wijnandts van Resandt, Th. van Dijk, S. Doorn and H. H. Roukens.

This work is part of the research program of the Stichting voor Fundamenteel Onderzoek der Materie (Foundation for Fundamental Research on Matter) and was made possible by financial support from the Nederlandse Organisatie voor Zuiver-Wetenschappelijk Onderzoek (Netherlands Organization for the Advancement of Pure Research).

REFERENCES

1) de Heer, F. J., van Eck, J., and Kistemaker, J., (1963), Proc. 6th Intern. Conf. Ionization Phenomena in Gases, Paris, 1963, Vol. I, pp. 73–76, Editors P. Hubert and E. Cremieu-Alcan, Centre de Documentations Universitaires (Paris).
2) Head, C. E. and Hughes, R. H., Phys. Rev. **139** (1965) A1392.
3) de Heer, F. J., Wolterbeek Muller, L. and Geballe, R., Physica **31** (1965) 1745.
4) Dworetsky, S. H., Novick, R., Smith, W. W. and Tolk, N., Phys. Rev. Letters **18** (1967), 939; Dworetsky, S. H. and Novick, R., Phys. Rev. Letters **23** (1969) 1484.
5) Dworetsky, S. H., Novick, R. and Tolk, N., ICPEAC VI (1969) 294, MIT Press (Cambridge, Massachusetts).
6) Tolk, N. and White, C. W., ICPEAC VI (1969) 309, MIT Press (Cambridge, Massachusetts).
7) Gilbody, H. G., Browning, R., Levy, G. J., McIntosh, A. I. and Dunn, K. G., J. Phys. **B**: Atom. Mol. Phys. **1** (1968) 863.
8) Miers, R. E., Schlachter, A. S. and Anderson, L. W., Phys. Rev. **183** no. 1 (1969) 213.
9) Peterson, J. R. and Lorents, D. C., Phys. Rev. **182** no. 1 (1969) 152.
10) de Heer, F. J. in "Advances in Atomic and Molecular Physics", vol **2** (1966) 327, Editors D. R. Bates and I. Esterman, Academic Press, (New York).
11) van Eck, J., de Heer, F. J. and Kistemaker, J., Physica **30** (1964), 1171.
12) van den Bos, J., Winter, G. J. and de Heer, F. J., Physica **40** (1968), 357.
13) Ishii, H. and Nakayama, K., Proc. 8th National Vacuum Symposium (1961) 519.
14) de Heer, F. J., Schutten, J. and Moustafa Moussa, H. R., Physica **32** (1966) 1766.
15) de Vos, J. C., thesis, Vrije Universiteit Amsterdam, 1953.
16) Wolterbeek Muller, L., The absolute calibration of a 2600–7000 Å spectrograph with photomultiplier. FOM-rep. 19353.
17) Krefft, H., Rössler, F. and Rüttenauer, A., Z. techn. Phys. **18** (1937) 20.
18) van Stekelenburg, L. H. M., Rapport no. 5, Afd. Gezondheidstechniek T.N.O., July 1951.
19) Hanle, W. and Voss, G. A., Z. Naturforsch. **11A** (1956) 857.
20) Trefftz, E., Schlüter, A., Dettman, K. H. and Jörgens, K., Z. Astrophysik **44** (1957) 1.
21) Gabriel, A. H. and Heddle, D. W. O., Proc. Roy. Soc. **A258** (1960) 124.
22) Dalgarno, A. and Lynn, N., Proc. Phys. Soc. **A70** (1957) 802.
23) Dalgarno, A. and Stewart, A. L., Proc. Phys. Soc. **74** (1957) 49.
24) Bates, D. R. and Damgaard, A., Phil. Trans. London **A212** (1949) 101.
25) Schiff, B. and Pekeris, C. L., Phys. Rev. **134** (1964) A638.
26) Weiss, A. W., J. Res. Nat. Bur. Stand. **71A** no. 2 (1967) 163.
27) Smit, J. A., Physica II **2** (1935) 104.

28) Thomas, E. W., Edwards, J. L. and Ford, J., ICPEAC VI (1969) 462, MIT Press, (Cambridge, Massachusetts).
29) de Heer, F. J. and van den Bos, J., Physica **31** (1965) 365.
30) Scharmann, A. and Schartner, K. H., Z. Phys. **228** (1969) 254.
31) Bell, K. L., Kennedy, D. J. and Kingston, A. E., J. Phys. **B**: Atom. Mol. Phys. **1** (1968) 1037.
32) Oldham, W. J. B., Phys. Rev. **174** no. 1 (1968) 145.
33) van den Bos, J., Phys. Rev. **181** (1969) 181.
34) Dodd, J. G. and Hughes, R. H., Phys. Rev. **135** (1964) A618.
35) Massey, H. S. W., Rep. Progr. Physics **12** (1949) 248.
36) Hasted, J. B., Advances Electron. Electron Physics **13** (1960) 1.
37) Solev'ev, E. S., Ill'in, R. N., Oparin, V. A. and Fedorenko, N. V., Soviet Physics-JETP **15** (1962) 459.
38) Pretzer, D., van Zijl, B. and Geballe, R., (1964), Third ICPEAC, London, 1963, p. 618, North-Holland Publ. Co. (Amsterdam).
39) Jaecks, D., van Zijl, B. and Geballe, R., Phys. Rev. **137** (1965) A340.
40) Bates, D. R. and Dalgarno, A., Proc. Phys. Soc. **A66** (1953) 972.
41) van den Bos, J. and de Heer, F. J., Physica **34** (1967) 333 and **40** (1968) 161.
42) Marchi, R. P. and Smith, F. T., Phys. Rev. **139** (1965) A1025.
43) Allab, D., Barat, M. and Baudon, J., J. Physique **29** (1968) 111.
44) Lichten, W., Phys. Rev. **131** (1963) 229.
45) Lockwood, G. J. and Everhart, E., Phys. Rev. **125** (1962) 567.
46) Smith, F. J., Phys. Rev. Letters **20** (1965) 271.
47) Lorentz, D. C. and Aberth, W., Phys. Rev. **139** (1965) A1017.
48) Lockwood, G. J., Helbig, H. F. and Everhart, J., Phys. Rev. **132** (1963) 2078.
49) Lorentz, D. C., Aberth, W. and Hesterman, V. W., Phys. Rev. Letters **17** (1966) 849.
50) Baudon, J., Barat, M. and Abignoli, M., J. Phys. **B**: Atom. Mol. Phys. **3** (1970) 207.
51) Coffey, D., Lorents, D. C. and Smith, F. T., Phys. Rev, 187 no. 1 (1969) 201.
52) Smith, F. J., ICPEAC V (1967) 177, Editors I.P. Flaks and E.S. Solovyov, Publishing House Nauka, Leningrad.
53) Smith, F. J., ICPEAC VI (1969) 1068, M.I.T. Press (Cambridge, Massachusetts).
54) Perel, J., Vernon, R. H. and Daley, H. L., Phys. Rev. **138** (1965) A937.
55) Rosenthal, H. and Foley, H. M., Phys. Rev. Letters **23** (1969) 1480.
56) Sural, D. P. Mukherjee, S. C. and Sil, N. C., Phys. Rev. **164** (1967) 156.
57) Wilets, L. and Gallaher, D. F., Phys. Rev. **147** (1966) 13.
58) Michels, H. H., in N.B.S. Technical Note 438, 1967. Compendium of ab initio calculations of Molecular Energies and Properties by Morris Kraus.
59) Lichten, W., Phys. Rev. **164** (1967) 131.

CHAPTER III

IONIZATION OF EXCITED HELIUM ATOMS INCIDENT ON SOME NOBLE GASES AT 90 keV

In section 10 of Chapter II a brief description was given of a pressure effect in the determination of the emission cross sections for radiative capture by helium ions incident on noble gases. It was found that above a certain pressure the radiation intensity emitted by the beam ceased to be proportional with the target gas density. In all cases investigated this effect caused the line intensity to be less than proportional with the target pressure (see fig. 9 of Chapter II). This deviation was found to increase with the lifetime of the upper level of the relevant transition and with the distance covered by the beam in the target gas.

Possible causes leading to such an effect are:

A. Decrease of the number of beam ions available for capture of an electron into the relevant excited state:
   1 - by scattering over an angle outside the optical observation region;
   2 - by electron capture to final states different from the state under consideration.

B. Loss of beam atoms which have been formed in the relevant excited state by electron capture:

1 - by transfer to another excited state;

2 - by loss of an electron (ionization of the excited atom).

The pressure effect was found to be relatively strong at 90 keV impact energy, where it was studied in more detail. At this energy the scattering is strongly forwardly directed and does not play a role. The total electron capture has already passed its maximum cross section at lower energies. Therefore the pressure effect must be mainly due to the processes mentioned under B. Electric and magnetic quenching of atomic states can be excluded in the case of helium, because the fields would have had to be very large. On the basis of these conclusions we are able to calculate cross sections for ionization of the excited atoms from pressure dependent measurements of the line emission by the excited helium atoms in the beam. We proceed as follows:

As far as possible the symbols to be used are the same as in section 2 of Chapter II. For the study of the pressure dependence of the transitions between the levels i and j we consider as the relevant states of the beam particles: i and j, being the upper and lower level of the radiative transition of consideration, O, being all possible atomic states except i, and +, the ionic state. The relevant cross sections then are:

σ_{+i} the cross section for the transition from the ionic state to the excited state i of the neutral atom,

σ_{+o} the charge exchange cross section, assuming the contribution of charge exchange to state i to be negligible with respect to the electron capture to all

other states,

σ_{i+} the cross section for ionization of the atom in state i.

Population of state i by cascade from higher states is neglected.

$n_i(x)$ and $n_+(x)$ are the number of beam particles per cm being in state i and the ionic state, respectively.

The decrease of the number of ions in the beam, caused by the charge exchange, is given by the equation:

$$dn_+(x) = - n_+(x)\ \sigma_{+o} N\ dx,$$

N is the target gas density in cm^{-3}.

Integration gives

$$n_+(x) = n_+(0)\ \exp(-\sigma_{+o} Nx) = \frac{1}{v}\frac{I_B}{e}\exp\ (-\sigma_{+o} Nx).$$

$\frac{I_B}{e}$ is the flux of beam ions at the entrance of the chamber, v their velocity.

According to our considerations we put the rate of population of states i among the beam particles equal to the algebraic sum of creation of states i by electron capture and of destruction by spontaneous radiative decay and by ionization in secondary collisions:

$$dn_i(x) = n_+(x)\ \sigma_{+i} N\ dx - n_i(x)\ \frac{dx}{v\tau_i} - n_i(x)\ N\ \sigma_{i+} dx.$$

As has been stated before, the contribution by cascade is neglected. τ_i is the radiative lifetime of state i.

From this differential equation we get after some operation:

$$n_i(x) = \frac{1}{v}\frac{I_B}{e}\frac{\sigma_{+i}N}{(\sigma_{i+}-\sigma_{+o})N+\frac{1}{x_i}}\left(e^{-\sigma_{+o}Nx} - e^{-(\sigma_{i+}N+\frac{1}{x_i})x}\right),$$

where $x_i = v\tau_i$.

From this result we derive the influence of the target density N on the emission of the radiation $i \to j$ as observed. The number of photons $i \to j$ emitted per second in the region of observation at distance L from the entrance opening will be, according to eq. (4) from section 2 of Chapter II.

$$S_{i\to j} = \int_1^{1+L} n_i(x)\, A_{ij}\, dx =$$

$$= \frac{\frac{1}{v}A_{ij}\frac{I_B}{e}\sigma_{+i}N}{-\sigma_{+o}N+\sigma_{i+}N+\frac{1}{x_i}} \times$$

$$\left[\frac{e^{-\sigma_{+o}N1}}{\sigma_{+o}N}\left(1-e^{-\sigma_{+o}NL}\right) - \frac{e^{-(\sigma_{i+}N+\frac{1}{x_i})1}}{\sigma_{i+}N+\frac{1}{x_i}}\left(1-e^{-(\sigma_{i+}N+\frac{1}{x_i})L}\right)\right]$$

This calculation is analogous to the one carried out by Edwards and Thomas[1] for the process of loss of excited hydrogen atoms colliding with gases. Developping the exponential terms into powers of N and retaining only the first and second order term one obtains after straightforward operation:

$$S_{i\to j} = a\,[bN - (c\sigma_{i+} + d\sigma_{+o})N^2]$$

in which

$$a = A_{ij}\,\frac{I_B}{e}\,\sigma_i\,\tau_i\,L$$

$$b = 1 - \frac{x_i}{L}\,e^{-\frac{1}{x_i}}\,(1 - e^{-\frac{L}{x_i}})$$

$$c = x_i + x_i\,e^{-\frac{1+L}{x_i}} - \frac{x_i}{L}\,e^{-\frac{1}{x_i}}\,(1 - e^{-\frac{L}{x_i}})(2x_i + L)$$

$$d = -x_i + 1 + \tfrac{1}{2}L + \frac{x_i}{L}\,e^{-\frac{1}{x_i}}\,(1 - e^{-\frac{L}{x_i}})\,x_i.$$

The magnitude of the constant of proportionality **a** is not relevant. b, c and d depend, apart from the chamber geometry, on the radiative lifetime only and can be calculated as these quantities are rather well known for helium. In b one recognises the correction factor for emission by fast excited atoms due to the lifetime of the excited state, first described by Hanle and Voss[2] and, in a more complicated form, applied in Chapter II.

The relative dependence of the emission $S_{i\to j}$ on the target gas density N has been measured. The coefficient of N^2, $\frac{c}{b}\,\sigma_{i+} + \frac{d}{b}\,\sigma_{+o}$, is the slope of the curve of $S_{i\to j}$ plotted against N. For σ_{+o} the values of de Heer et al.[3] have been inserted. Measurements have been carried out at 90 keV acceleration energy for some excited states of He in the case of He^* incident on Ar, Kr and Xe.

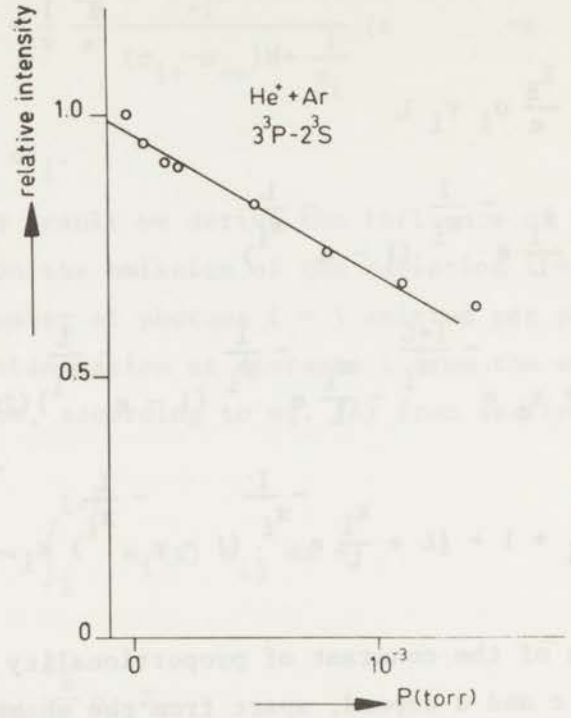

Fig.1. Emission of He ($3^3P - 2^3S$) radiation by collision of helium ions on argon, as a function of argon pressure.

As far as relevant our data are compared with recent data of Gilbody et al.[4], who measured electron loss cross sections by ground state and metastable helium atoms colliding on noble and some other gases, except xenon.

Due to the complicated evaluation of the data from the measurements a large error in the present results can be expected, of the order of 40%. Despite of this, comparison with the data of ref. 4 shows clearly a very strong increase of the electron loss process with decreasing bin-

TABLE I

Cross sections for electron loss by helium atoms in the ground state, metastable states and excited states colliding on noble gases at 90 keV.

	σ_{o+} ground state (10^{-17} cm^2) (see ref.4)	σ_{o*+} metastable (10^{-17} cm^2) (see ref.4)	σ_{i+} excited (10^{-17} cm^2) (this work)	
He on Ar	21	130	570	(3^3P)
			410	(4^1D)
			600	(4^3S)
			700	(4^3P)
			900	(5^3S)
He on Kr	17	160	650	(4^1S)
			550	(5^3S)
He on Xe			920	(4^1S)
			1000	(4^3S)
			960	(5^3S)

ding energy of the electron. From this reasoning one might further expect that within the present measurements a relation between the loss cross sections and the quantum states could be derived. In the argon data there is an indication that the cross section values increase with head quantum number, but this is not confirmed by the krypton and xenon results. This is probably due to the relatively small differences in binding energy between the

n = 3,4,5 states compared to n = 2 and the ground state and to the spread in the measurements. In the classical picture, however, the orbit of the outer electron describes an area proportional to n^4, from which one would expect a knocking-off collision cross section to rise steeply with n.

REFERENCES

1) Edwards, J.L. and Thomas, E.W., Phys.Rev. A2 (1970) 2346.

2) Hanle, W. and Voss, G.A., Z.Naturforsch. 11A (1956) 857.

3) de Heer, F.J., Schutten, J. and Moustafa, H., Physica 32 (1966) 1793.

4) Gilbody, H.B., Dunn, K.F., Browning,R. and Latimer, C.J., J.Phys.B.: Atom.Molec.Phys. 3 (1970) 1105.

SUMMARY

In this thesis we describe an experimental study on the capture of electrons by helium ions incident on noble gas atoms, where the electron is transferred from the target atom to an excited state of the projectile (helium) atom. These excited states give rise to emission of photons, thus decaying to lower excited states or the ground state of the helium atom. By measuring the intensity of the photons it is possible to determine the relevant cross sections for electron capture into excited states.

In Chapter I a general introduction and literature review are given.

In Chapter II our own experiment is discussed. The He^+ ions in this work are accelerated between 300 eV and 150 keV, by means of three different ion accelerators. One of these, developped in the course of this experiment for energies between 2 and 40 keV, is described in more detail. The excited states for which electron capture cross sections have been determined are singlet and triplet S, P and D states of He with n = 3,4,5 and 6. Further for the case of He^+ incident or He, direct excitation of the target atom was also measured in order to compare capture and excitation processes leading to the same excited state of He, either of the projectile or the target atom.

In the experiment particular attention was given to the different factors which may influence the intensity measurement as: finite lifetime of the excited atom, polarization of the radiation, Doppler broadening of the emission lines and pressure effects due to ionization of the

excited fast atom in a second collision. In the evaluation of the excitation processes, also the effect of cascade from higher excited levels was taken into account.

In all the cross sections a maximum was found at an impact energy that can be correlated to the so called criterion of Massey. This criterion predicts a resonance (maximum) in the cross section when the effective collision time $\tau = \frac{a}{v}$ (a = effective interaction distance, v = relative velocity) is of the same order of magnitude as the reverse of the transition frequency $\nu = \frac{\Delta E}{h}$ (ΔE = change of internal energy). The main maximum is reached between about 50 and 130 keV, ΔE varies from about 22 eV in the case of He^+ on He to 10 eV in the case of He^+ on Xe, corresponding to **a** values between 3 and 7 Å. This is of the same order of magnitude as has been found for other collision processes like electron capture into the ground state, ionization and direct excitation.

Below this maximum, however, several other maxima were found. This is connected with the formation of an intermediate molecular complex, possibly with pseudocrossing of potential curves. This mechanism gives rise to a smaller effective value of **a** ΔE than used in Massey's criterion where only initial and final atomic states of the collision products are taken into account. Some more remarks about these maxima and consequently oscillations in the cross sections are given further on. They can be qualitatively explained in terms of a two state approximation, where the collision process occurs via two different channels, leading to interference effects.

At the higher part of the energy impact region (above

about 60 keV), the cross sections are systematically larger the heavier the target atom. As to the dependence of the azimuthal quantum number, it is found that the decrease of the cross section past the main maximum is faster for the D states than for the P and S ones for increasing impact energy. The difference between S and P capture is not so clear in this energy range. The relatively fast decrease for the D state is in agreement with theory which predicts a relatively faster decrease at high impact energies for levels with larger angular momentum.

For He^+ on He oscillations in the cross section are found both for excitation and electron capture. For identical excited states the oscillations for excitation and capture are almost in phase at the lower impact energies, in antiphase at the higher energies. At low impact energies it is assumed that these excited states are formed via a curve crossing of the two gerade states of the He_2^+-ion because no curve crossing exists for the relevant ungerade states. This leads to the oscillations in phase for excitation and capture. The experimental evidence for antiphase oscillations at high impact energies indicates that excitation should take place to a gerade as well as to an ungerade state of the molecular ion. Then by interference this leads to antiphase oscillations in capture and excitation.

The oscillations presented in this work are due to a different mechanism as considered in the experiments of Dworetsky et al. (ref.3 and 4 of Chapter II). Oscillations are also found for the total cross sections of electron capture (into excited states) in the case of He^+

on Ne, Ar, Kr and Xe. This may be explained by curve crossing of two states of the $(HeX)^+$ molecular ion where X stands for the noble gas atom.

In Chapter III a process is described that gives to an unexpectedly great pressure effect in our electron capture measurements as shown in Chapter II. It was concluded that this was due to the large electron loss cross section for excited beam atoms travelling through the target gas. Their excitation energy is relatively close to the ionization energy so that little energy is needed for the electron loss process. From measurements of the pressure dependence of the light emission for several excited states cross sections for electron loss at 90 keV could be evaluated and were compared with data for ionization of ground state and metastable helium atoms.

SAMENVATTING

In dit proefschrift wordt een experimenteel onderzoek beschreven betreffende electronvangst door heliumionen bij botsing op edelgasatomen, waarbij een electron van het doelwitatoom naar een aangeslagen toestand van het projectiel (atoom) wordt overgedragen. Deze aangeslagen toestanden leiden tot het uitzenden van fotonen, waarbij het projectiel naar lagere energietoestanden of naar de grondtoestand van het heliumatoom terugvalt. Door meting van de fotonenemissie kan men de botsingsdoorsneden bepalen, die betrekking hebben op de vangst van het electron naar aangeslagen toestanden.

In Hoofdstuk I worden een algemene inleiding en literatuuroverzicht gegeven.

Hoofdstuk II begint met een beschrijving van het experiment. De He^+ ionen worden versneld met energieën tussen 300 eV en 150 keV met behulp van drie verschillende versnellers. Een daarvan, ontwikkeld tijdens het onderzoek, werkt in het gebied van 2 en 40 keV en wordt beschreven.

De aangeslagen toestanden, waarvoor de vangstdoorsneden werden bepaald, zijn de singlet en triplet S, P en D toestanden van He met n = 3,4,5 en 6. Voorts is er in het geval van He^+ botsend op He ook directe aanslag van het doelwitatoom gemeten om een vergelijking te kunnen maken tussen vangst- en aanslagprocessen leidend tot dezelfde aangeslagen toestand van He, hetzij van het projectiel, hetzij van het getroffen atoom.

Bij het onderzoek werd aandacht besteed aan verscheidene oorzaken, die de intensiteitsmeting van fotonen kunnen

beïnvloeden, zoals: de eindige levensduur van de aangeslagen toestand, polarisatie van de straling, Dopplerverbreding van de spectraallijnen en drukeffecten, veroorzaakt door ionisatie van het aangeslagen snelle atoom in een tweede botsing. Bij de uitwerking van de metingen aan aangeslagen niveau's werd ook het effect van de zogenaamde cascade, de bijdrage afkomstig van terugval uit hogere niveau's, in rekening gebracht.

Bij alle botsingsdoorsneden werd een maximum in de energie-afhankelijkheid gevonden, dat in verband gebracht kan worden met het zogenaamde kriterium van Massey. Dit kriterium voorspelt een resonantiemaximum in de botsingsdoorsnede, wanneer de effectieve botsingstijd $\tau = \frac{a}{v}$ (a = effectieve wisselwerkingsafstand, v = relatieve snelheid) van dezelfde orde van groote is als het omgekeerde van de overgangsfrequentie $\nu = \frac{\Delta E}{h}$ (ΔE = verschil in inwendige energie vóór en na de botsing). Het hoofdmaximum wordt bereikt tussen ongeveer 50 en 130 keV, ΔE varieert van ongeveer 22 eV bij He^+ op He tot 10 eV voor He^+ op Xe, wat overeenkomt met waarden voor **a** van 3 tot 7 Å. Dit is van dezelfde orde van grootte als werd gevonden voor andere botsingsprocessen zoals electronvangst naar de grondtoestand, ionisatie en directe aanslag.

Beneden dit maximum werden echter nog meer maxima gevonden. Dit hangt samen met de tijdelijke vorming van een moleculair complex, mogelijk samen met zogenaamde pseudocrossing van potentiaalkrommen. Dit mechanisme veroorzaakt een kleinere effectieve waarde van **a** ΔE dan genomen wordt in het kriterium van Massey, waarbij alleen begin- en eindtoestanden van de atomaire botsingsproducten in

rekening worden gebracht. Er worden enkele opmerkingen gemaakt in verband met deze maxima en daarmee samenhangende oscillaties in de botsingsdoorsneden. Deze kunnen kwalitatief verklaard worden met het model van een twee-toestandsbenadering, waarbij de botsing plaats kan vinden via twee verschillende wegen, wat leidt tot interferentie effekten.

Aan de hoge energiezijde van het meetgebied (boven ongeveer 60 keV) zijn de botsingsdoorsneden groter met zwaarder doelwitatoom. Wat betreft de afhankelijkheid van het azimuthale kwantumgetal is gevonden, dat de afname van de doorsneden voorbij het hoofdmaximum sneller is voor de D-toestanden dan voor P en S. Het verschil tussen S en P is niet zo duidelijk in dit energiegebied. Het relatief snelle afnemen van de D-toestand is in overeenstemming met de theorie, die een snellere daling met de botsingsenergie voorspelt voor doorsneden van toestanden met groter impulsmoment.

Voor He^+ op He werden oscillaties gevonden, zowel voor directe aanslag als voor electronvangst. Bij dezelfde toestanden zijn de oscillaties voor directe aanslag en voor vangst in aangeslagen toestand ongeveer in fase bij lage energieën en in tegenfase bij hogere. Bij lage botsingsenergieën wordt aangenomen, dat deze aangeslagen toestanden gevormd worden via kruising van potentiaalkrommen van de beide even toestanden van het He_2^+-ion, omdat oneven potentiaalkrommen elkaar niet kunnen kruisen. Dit leidt tot het in fase zijn van de botsingsdoorsneden voor aanslag en vangst naar dezelfde toestand. Het experimentele resultaat van de oscillaties die in tegenfase zijn

geeft een aanwijzing dat directe aanslag plaatsvindt zowel naar een even als naar een oneven toestand. Door interferentie leidt dit tot tegenfase oscillaties in vangst en directe aanslag.

De oscillaties, weergegeven in dit werk, zijn afkomstig van een ander mechanisme dan wat in het werk van Dworetsky en anderen in beschouwing werd genomen. Ook werden oscillaties gevonden voor botsingsdoorsneden voor electronvangst (naar aangeslagen toestanden) voor He^+ op Ne, Ar, Kr en Xe. Dit kan wellicht verklaard worden door kruising van potentiaalkrommen van twee toestanden van het $(HeX)^+$-molecuul waarbij X het edelgasatoom voorstelt.

In Hoofdstuk III wordt een proces beschreven, dat een onverwacht groot drukeffect gaf in de electronvangstmetingen. Er werd de conclusie getrokken, dat dit zijn oorzaak vond in de zeer grote doorsnede voor electronverlies voor aangeslagen He-bundelatomen, die door het botsingsgas vliegen. De aanslagenergie verschilt weinig van de ionisatie-energie, zodat er weinig energie nodig is voor electronverlies. Uit metingen van drukafhankelijkheden van de lichtemissie voor verscheidene aangeslagen toestanden konden doorsneden voor electronverlies worden berekend. Dit is gedaan bij 90 keV, waar het effect ongeveer het grootst was. De resultaten worden vergeleken met die voor ionisatie van helium in de grondtoestand en in de metastabiele toestand.

Volgens het gebruik in de Faculteit der Wiskunde en Natuurwetenschappen volgt hier een kort overzicht van mijn studie.

Na het behalen van het einddiploma B aan het Gymnasium Haganum te Den Haag begon ik in 1954 met de studie in de wis- en natuurkunde aan de Rijksuniversiteit te Leiden. Het kandidaatsexamen a' werd afgelegd in oktober 1958, waarna de studie werd voortgezet in de experimentele natuurkunde. Daarbij heb ik deel uitgemaakt van de groep paramagnetische relaxatie onder leiding van Dr J.C. Verstelle. Het doctoraalexamen met bijvakken mechanica en electronica volgde in mei 1962.

Hierna kwam ik als wetenschappelijk medewerker in dienst bij het F.O.M.-Instituut voor Atoom- en Molecuulfysica te Amsterdam, toen nog Laboratorium voor Massascheiding geheten, onder leiding van Professor Dr J. Kistemaker. Van mei tot augustus 1962 heb ik daar gewerkt in de groep Thermonucleaire Reacties III onder leiding van Dr F.G. Insinger.

Na de militaire dienst, gedurende welke ik werkte in de afdeling Reactorkunde bij het Technisch Documentatie- en Informatie Centrum voor de Krijgsmacht, keerde ik in mei 1964 terug op het F.O.M.-Instituut, dit maal in de groep Atomaire Botsingen onder leiding van Dr F.J.de Heer. Hier heb ik een onderzoek gedaan over electronvangst bij ion-atoombotsingen, n.l. waarbij een electron overgaat van het doelwitatoom naar het projectiel ion en in een aangeslagen toestand komt van het (projectiel) atoom. Dit

onderzoek wordt in dit proefschrift beschreven. Verder deed ik metingen met ver-ultraviolette optiek aan aanslag van edelgasatomen door helium-ionen en aan Lyman-α emissie bij botsing van protonen op edelgassen en verrichtte absoluut ijking van optische detectors.

Van februari 1969 tot mei 1970 was ik "visiting scientist" aan het European Space Research Institute in Frascati (Roma), Italie, in de groep Ion Physics, waar ik gewerkt heb aan het opwekken van een bundel volledig geioniseerde koolstofatomen met behulp van lasertechnieken.

In mei 1970 ben ik in dienst gekomen van de groep Kwantumelectronica aan de Technische Hogeschool Twente.

Het was mij een grote voldoening bij Professor Dr J. Kistemaker en Dr F.J.de Heer te hebben mogen werken. Het telkens bereid zijn van Dr F.J.de Heer mij bij te staan bij problemen van het onderzoek heb ik ten zeerste gewaardeerd. Bij de metingen werd ik op waardevolle wijze bijgestaan door Drs B.F.J. Luyken, Drs R.H.J. Jansen en verder door de heren Th.van Dijk, J.B.M.van Dijk, R.W. Wijnandts van Resandt en H. Marsman. Bij de apparatuur werd steun verleend door de heren E.de Haas en A.F. Neuteboom wat constructie en de heren P.van Deenen en J. Keizer wat electronica betreft. Hen dank ik hiervoor en tevens de heren F. Monterie en, wederom, Th.van Dijk voor het fotografische werk, alsmede Mevr. G.A.M.van der Voort-van Dorsselaer voor het typewerk.

STELLINGEN

1. Het berekenen van botsingsdoorsneden voor de bevolking van aangeslagen toestanden uit stralingsmetingen, zonder kennis van de orde van grootte van de bezetting van naburige termseries, kan soms tot een fout van een factor 3 leiden.
   Dit proefschrift, hoofdstuk II.

2. Bij drukafhankelijke bepaling van levensduren van aangeslagen toestanden van atomen of moleculen in een gas kan extrapolatie naar de lage-druklimiet een onjuiste waarde voor de natuurlijke levensduur geven.
   Jansen, R.H.J., FOM-rapport no. 29804 (1970).
   Fink, E en Welge, K.H., Z. Naturforschung 19a (1964), 1193 en 23a (1968), 358,
   Bennett, R.G. en Dalby, F.W., J. Chem. Phys. 31 (1959), 434.

3. Er bestaat een sterke configuratiewisselwerking binnen de $3p^4nd$-serie van Ar II, in tegenstelling tot de $3p^4np$-serie. Dit geldt ook voor de overeenkomstige configuraties van Ne II, zij het in mindere mate.
   Luyken, B.F.J., Physica 51 (1971), 445.

4. De opmerking van Newton en Sciamanna, dat de $C^2\Sigma_u^+$ toestand van N_2^+ een levensduur $< 10^{-7}$ sec. moet hebben, omdat deze toestand een toegestane overgang naar de grondtoestand heeft met een golflengte in het vacuüm-u.v.-gebied, is ongegrond.
   Newton, A.S. en Sciamanna, A.F., J. Chem. Phys., 50 no. 11 (1969), 4868.

5. Voor de bepaling van accommodatiecoëfficiënten van snelle moleculen, die botsen op metaaloppervlakken wordt door Devienne een calorische methode gebruikt. Ten onrechte wordt daarbij als warmtelek alleen de uitstraling genomen.
   Devienne, F.M., Int. J. Heat Mass Transfer 10 (1967), 1109.

6. De electronentemperatuur van een plasma van lichte ionen in het gebied van 100 eV en hoger kan goed gemeten worden door gebruik te maken van de emissie van remstraling. Annname van de Boltzmannverdeling voor de electronen is hiervoor noodzakelijk. Dat daaraan voldaan wordt, ondanks ionisatieprocessen , kan aannemelijk worden gemaakt.
   Wolterbeek Muller, L. en Green, T.S., Plasma Phys. 13 (1971), 73.

7. De drie-deeltjesrecombinatie in een uitdijend plasma wordt tegengewerkt door de vrijkomende elecronenenergie. Dit wordt niet altijd voldoende in rekening gebracht.
   Gurevich, A.V. en Pitaevski, L.P., J.E.T.P. 19, (1964), 795.

8. Bij de metingen van Moustafa en de Heer, waarbij electronen op heliumatomen geschoten worden, is de systematische verandering van de verhouding van de intensiteiten van de He II-emissielijnen van 4686 Å en 1216 Å bij botsingsenergieën < 250 eV waarschijnlijk veroorzaakt door verontreinigingen in het helium-gas, van enkele duizendsten.
   Moustafa Moussa, H.R., en de Heer, F.J., Physica 34 (1967), 646 en 50 (1969), 1863.
   Vroom, D.A. en de Heer, F.J., J. Chem. Phys. 50 (1969), 573 en 580.

9. De mogelijkheden van het verstemmen van lasersystemen met een tralie in de zgn. Littrowopstelling kunnen aanzienlijk worden vergroot door het toevoegen van een breedbandige reflector en door gebruik te maken van de coherentieëigenschappen van laserstraling.

10. Er zijn aanwijzingen, dat een hoog-vermogen CO-laser met een rendement van meer dan 10 % niet alleen in doorstroomsystemen bij cryogene temperaturen, maar ook in afgesloten systemen bij kamertemperatuur kan worden verkregen. Het inversiemechanisme

is waarschijnlijk niet cascade vanuit hogere electrontoestanden van CO, zoals gesuggereerd wordt door Patel.

Patel, C.K.N., Phys. Rev. 141 (1966), 71.

11. Bij parlementsverkiezingen volgens een districtenstelsel wordt het beginsel "one man, one vote" slechts in schijn toegepast.